online data

Neuropilin-1 regulates platelet-derived growth factor receptor signalling in mesenchymal stem cells

Stephen G. BALL, Christopher BAYLEY, C. Adrian SHUTTLEWORTH and Cay M. KIELTY[1]

Wellcome Trust Centre for Cell-Matrix Research, Faculty of Life Sciences, University of Manchester, Manchester M13 9PT, U.K.

Using human MSCs (mesenchymal stem cells) lacking VEGF (vascular endothelial growth factor) receptors, we show that the pro-angiogenic receptor neuropilin-1 associates with phosphorylated PDGFRs [PDGF (platelet-derived growth factor) receptors], thereby regulating cell signalling, migration, proliferation and network assembly. Neuropilin-1 co-immunoprecipitated and co-localized with phosphorylated PDGFRs in the presence of growth factors. Neuropilin-1 knockdown blocked PDGF-AA-induced PDGFRα phosphorylation and migration, reduced PDGF-BB-induced PDGFRβ activation and migration, blocked VEGF-A activation of both PDGFRs, and attenuated proliferation. Neuropilin-1 prominently co-localized with both PDGFRs within MSC networks assembled in Matrigel™ and in the chorioallantoic membrane vasculature microenvironment, and its knockdown grossly disrupted network assembly and decreased PDGFR signalling. Thus neuropilin-1 regulates MSCs by forming ligand-specific receptor complexes that direct PDGFR signalling, especially the PDGFRα homodimer. This receptor cross-talk may control the mobilization of MSCs in neovascularization and tissue remodelling.

Key words: co-localization, mesenchymal stem cell, migration, network assembly, neuropilin-1, platelet-derived growth factor receptor.

INTRODUCTION

MSCs (mesenchymal stem cells) in bone marrow and perivascular niches throughout the body are reservoirs of multipotent cells that can differentiate along mesenchymal lineages, including smooth muscle, and undergo endothelial transdifferentiation in response to VEGF (vascular endothelial growth factor) [1–3]. We have previously shown that multipotent human MSCs express NRP-1 (neuropilin-1) and PDGFRs [PDGF (platelet-derived growth factor) receptors] α and β, but not VEGFRs (VEGF receptors), and that both PDGFs and VEGF-A stimulate PDGFRs thereby regulating proliferation, migration and smooth muscle-specific cytoskeleton [2,4].

NRP-1 is a type I transmembrane glycoprotein that regulates vascular and neural development and acts as a co-receptor for VEGFRs and plexins [5–11]. NRP-1-deficient or -overexpressing mice display severe abnormalities in nervous and cardiovascular systems [12,13], whereas NRP-1-null zebrafish have loss of circulation via angiogenic vessels [14]. The large extracellular region of NRP-1 comprises two CUB (complement binding) domains (designated a1a2), two coagulation factor V/VIII homology domains (designated b1b2) and a MAM (meprin, A5 antigen, receptor tyrosine phosphatase μ) domain (designated c). The last three C-terminal residues of NRP-1 form a PDZ-binding motif that influences NRP-1-mediated angiogenesis [15,16]. NRP-1 is highly expressed by numerous tumour cell lines, and enhances tumour survival, growth and vascularization *in vivo* [17–19].

In vascular endothelial cells, NRP-1 and the VEGFR2 co-cluster, but do not interact directly in the absence of VEGF-A_{165} [20,21]. NRP-1 b1b2 domains can bind the basic C-terminal tail of the heparan-sulfate-binding growth factor VEGF-A_{165}, which bridges extracellularly between VEGFR2 and NRP-1, generating a complex with enhanced VEGFR2 signalling that can induce angiogenic sprouting [7,22–26]. Cytoplasmic domains also contribute to VEGFR2–NRP-1 receptor complexes, since inhibiting VEGFR phosphorylation or deleting the PDZ domain of NRP-1 reduces this association [27]. In tumour cells that lack expression of VEGFR2, NRP-1 supports VEGF-mediated endothelial cell migration through PI3K (phosphoinositide 3-kinase)/Akt signalling, implying the existence of other receptors for NRP-1-mediated VEGF function [28,29]. Indeed, NRP-1 associates with heparan-sulfate-binding growth factors bFGF (basic fibroblast growth factor) and HGF (hepatocyte growth factor) [30], and can regulate HGF-induced c-met phosphorylation [31]. PDGF-B also influences vascular smooth muscle cell motility by up-regulating and associating with NRP-1 [32].

The PDGFR and VEGFR tyrosine kinases, and their growth-factor ligands, are closely related structurally and evolutionarily [33,34]. PDGFs induce receptor-specific activation, with PDGF-AA stimulating only PDGFR$\alpha\alpha$, whereas PDGF-BB stimulates all PDGFR dimers $\alpha\alpha$, $\beta\beta$ and $\alpha\beta$ [35]. PDGF-CC binds to PDGFRs $\alpha\alpha$ and $\alpha\beta$ [35], whereas PDGF-AB mainly signals through PDGFR$\alpha\beta$ [36]. In early embryonic development, PDGFRα and its major ligand PDGF-A are co-expressed from the two-cell stage, and PDGF-A-stimulated PDGFRα signalling is critical for differentiation of ES (embryonic stem) cells into mesenchymal, neural crest, cranial and myogenic cells, and for epithelial–mesenchymal transformation [37–39]. PDGF-A knockout is embryonic lethal, PDGFRα-null mice die during embryonic development, and mice null for PDGF-C die perinatally [34,40]. PDGFRs are also essential regulators of vessel-wall development [41] and remodelling following injury [42], with PDGF-B a major mitogenic and chemotactic ligand for smooth muscle cells and their mesenchymal precursors. NRP-1 expression also identifies vascular precursors in ES cells [43].

Abbreviations used: CAM, chorioallantoic membrane; DAPI, 4′,6-diamidino-2-phenylindole; ES, embryonic stem; HGF, hepatocyte growth factor; HUVEC, human umbilical vein endothelial cell; MSC, mesenchymal stem cell; NA, numerical aperture; NRP-1, neuropilin-1; p-, phosphorylated-; PDGF, platelet-derived growth factor; PDGFR, PDGF receptor; RT, reverse transcription; siRNA, small interfering RNA; VEGF, vascular endothelial growth factor; VEGFR, VEGF receptor.

[1] To whom correspondence should be addressed (email cay.kielty@manchester.ac.uk).

It was recently shown that bone marrow cells are recruited to sites of neovascularization through NRP-1 [44]. In the present study, using MSCs lacking VEGFRs, we show that NRP-1 co-localization with phosphorylated PDGFRs regulates their signalling in a ligand-specific manner, and has an indispensable role in PDGFRα-induced migration and MSC network assembly. This novel receptor cross-talk may thus control the recruitment of MSCs in vascular remodelling.

EXPERIMENTAL

Cell culture and reagents

Human MSCs from normal bone marrow of 20- and 26-year-old females and 18-, 22- and 24-year-old males (obtained from Lonza), were cultured on 0.1 % gelatine (Sigma–Aldrich) and maintained and characterized as described previously [45]. For each analysis, MSCs were analysed at passage 4. HUVECs (human umbilical vein endothelial cells) from 35- and 29-year-old females (Cascade Biologics) were maintained as described previously [45]. All growth factors were obtained from R&D Systems and VEGFR2 tyrosine kinase inhibitor V was supplied by Merck.

Flow cytometry

For single-colour flow cytometry, MSCs (4×10^6 cells/ml) were incubated with either PE (phycoerythrin)-conjugated anti-human NRP-1 (FAB3870P), VEGFR2 (FAB357P) or control anti-IgG_1 (IC002P) (R&D Systems) antibodies, then processed as described previously [2].

Immunofluorescence microscopy

MSCs were cultured on round glass coverslips in 24-well culture dishes, previously coated with 0.1 % gelatin overnight at 4 °C, or a thin-layer of growth-factor-reduced Matrigel™ (BD Biosciences) incubated at 37 °C for 30 min. Cells were fixed with 4 % (w/v) paraformaldehyde for 20 min, incubated in 0.2 M glycine for 20 min, then permeabilized using 0.5 % Triton X-100 in PBS for 4 min. After blocking in 2 % fish-skin gelatin in PBS (Sigma–Aldrich), pairs of primary antibodies in blocking solution (2 % fish-skin gelatin) were incubated overnight at 4 °C. Primary antibodies were all obtained from Santa Cruz Biotechnology: anti-human NRP-1 (sc-5541), NRP-1 (sc-7239), p-PDGFRα-Tyr^{754} (where p- indicates phosphorylated) (sc-12911), p-PDGFRα-Tyr^{720} (sc-12910), PDGFRα (sc-338), p-PDGFRβ-Tyr^{1021} (sc-12909-R), p-PDGFRβ-Tyr^{751} (sc-21902-R), p-Flk-1-Tyr^{1175} (sc-101819) and PDGFRβ (sc-339). Cells were then incubated with appropriate Alexa Fluor® 488 and Alexa Fluor® 555 fluorophores (Invitrogen) in blocking solution for 2 h at room temperature (20 °C) and coverslips were mounted on to glass slides with ProLong Gold antifade reagent with DAPI (4′,6-diamidino-2-phenylindole; Invitrogen). Images were collected with a Nikon C1 confocal microscope using a TE2000 PSF inverted microscope, utilizing 60 × /NA (numerical aperture) 1.40 Plan Apo or 20 × /NA 0.50 Plan Fluor objectives and 3 × confocal zoom. Different sample images detecting the same antibodies were acquired under constant acquisition settings. Images were processed using Nikon EZ-C1 FreeViewer v3.3 software. For co-localization analysis, images were processed using ImageJ software and a co-localization analysis plugin. For each analysed image, similar best-fit lower threshold values were determined to reduce the signal background of the corresponding red and green channels, then particle sizes for the red and green channels were set at a minimum of 1 pixel and maximum of 1000 pixels, then co-localization between channels was determined and represented by a yellow image.

Migration and proliferation assays

MSC migration was determined using a modified Boyden chamber assay as described previously [2]. The number of migratory MSCs on the membrane underside (cells/field using a 10 × /NA 0.3 UPlan F1 objective) were determined using an Olympus BX51 widefield microscope. Images were captured with a CoolSNAP camera system and processed using MetaMorph imaging v5.0 software. To determine proliferation, MSCs (2000 cells/well) in growth medium were seeded into 96-well plates coated with 0.1 % gelatin and incubated with or without PDGF ligands at 37 °C, with growth medium and ligands exchanged every 24 h. At the end of each time point, a CyQuant cell proliferation assay kit (Invitrogen) was used to detect MSC proliferation as described previously.

siRNA (small interfering RNA) transfections

MSCs (5×10^5 cells) together with 3 μg of siRNAs were transfected by electroporation using a human Nucleofector kit (Amaxa), then cultured for 20 h in growth medium at 37 °C in a humidified atmosphere of 5 % CO_2 in air. Two different validated siRNAs, functionally tested to provide $\geqslant$70 % target gene knockdown for NRP-1 were obtained from (i) Qiagen (S102663213) and (ii) Ambion (4390824) and a scrambled siRNA control was also obtained from Qiagen. The targeting specificity and efficiency following individual siRNA knockdowns was evaluated using primers and RT (reverse transcription)–PCR analysis, as described previously [2,45].

Immunoprecipitation analysis

MSC lysates were isolated as described previously [45], then 100 μg of lysate was incubated with antibodies against human NRP-1 (sc-7239), PDGFRα (sc-338) or PDGFRβ (sc-339) (Santa Cruz Biotechnology) overnight at 4 °C. Immune complexes were isolated by incubation with 10 % (w/v) protein A–Sepharose for 2 h, followed by immunoblot analysis as described previously [45], using antibodies against human PDGFRα (sc-338), PDGFRα-Tyr^{754} (sc-12911), PDGFRβ (sc-339), PDGFRβ-Tyr^{1021} (sc-12909) or NRP-1 (MAB38701) (R&D Systems). For quantification, the densities of bands were determined using Gene Tools software (Syngene), and normalization to the corresponding loading control.

Phosphorylated PDGFR immunoassays

A cell-based human p-PDGFRβ-Tyr^{751} ELISA kit (R&D Systems), was used to measure p-PDGFRβ-Tyr^{751} and modified to measure p-PDGFRα-Tyr^{742} utilizing an anti-p-PDGFRα-Tyr^{742} antibody (AF2114) (R&D Systems). MSCs (10 000 cells/well) in serum-free medium were seeded on to 0.1 % gelatin, stimulated with fresh serum-free medium containing a specific growth factor, then immediately analysed according to the manufacturer's protocol. The p-PDGFR fluorescence at 600 nm in each well was normalized to the total PDGFR fluorescence at 450 nm, and the means of triplicate readings were determined.

Matrigel™ network formation assay

Round glass coverslips were coated with a thin layer of growth-factor-reduced Matrigel™ (BD Biosciences), allowed to set, and then seeded with MSCs (2×10^4) in 0.5 % serum growth

medium and incubated at 37 °C. For quantification of network formation, the average number of branch points/field after 24 h was determined. Each assay was performed in duplicate, with the number of branch points/field counted from at least six random fields per well.

CAM (chorioallantoic membrane) *in vivo* angiogenesis assay

Briefly, fertilized White Leghorn chicken eggs were incubated at 38 °C for 5 days. Under aseptic conditions in a laminar flow cabinet, a small window at the top of the shell was carefully excised and the CAM blood vessels exposed. MSCs (2×10^4 cells) were seeded on to a Matrigel™-coated coverslip and incubated for 45 min at 37 °C to allow adherence. Coverslips were implanted MSCs face down on to a highly vascularized area of CAM, the shell opening sealed, and the MSCs incubated *in ova* at 38 °C for 24 h. Afterwards, coverslips were carefully removed from the CAM, washed in PBS and then processed for immunofluorescence microscopy.

Statistical analysis

In all quantification experiments, results are expressed as the means ± S.D. Statistical differences between sets of data were determined by using a paired Student's *t* test with SigmaPlot 8.0 software, with $P < 0.05$ considered significant.

RESULTS

PDGF ligands stimulated NRP-1 association with PDGFRs

We have previously shown that multipotential MSCs which express PDGFRs α and β, but no VEGFRs, on their cell surface, also expressed NRP-1 [2,4]. Using flow cytometry, we confirmed that MSCs express NRP-1 on their cell surface, but not VEGFR-2 (Figure 1A).

Co-immunoprecipitation experiments were conducted to examine whether NRP-1 associates with PDGFRα and/or PDGFRβ (Figure 1B). NRP-1 co-immunoprecipitated with PDGFRα, and vice versa, predominantly in the presence of its ligands PDGF-AA, PDGF-BB or VEGF-A_{165} [Figure 1B (i and iii)]. PDGFRβ and NRP-1 co-immunoprecipitated in the presence of PDGF-BB or VEGF-A_{165} [Figure 1B (ii and iv)]. These data demonstrate ligand regulation of the association of PDGFRs α and β with NRP-1.

To estimate the percentage of PDGFRs in a particular cell lysate which interact with NRP-1, co-immunoprecipitation analysis of total PDGFRs [Figure 1C (i and ii)] and phosphorylated PDGFRs [Figure 1C (iii and iv)] was evaluated. Using unstimulated control MSCs, co-immunoprecipitation analysis demonstrated $\sim 5.0 \pm 0.7$ % total PDGFRα or PDGFRβ associated with NRP-1 [Figure 1C (i and ii)], but MSC exposure to PDGF-AA resulted in 67 ± 8 % total PDGFRα being associated with NRP-1, while exposure to PDGF-BB induced 36 ± 7 % total PDGFRβ to associate with NRP-1 [Figures 1C (i and ii) and 1D (i)]. Similarly, co-immunoprecipitation analysis of PDGFRα phosphorylated at Tyr^{754} or PDGFRβ at Tyr^{1021} [Figure 1C (iii and iv)], demonstrated that unstimulated MSCs displayed $\sim 5.0 \pm 0.7$ % phosphorylated PDGFRs associated with NRP-1, whereas exposure to PDGF-AA or PDGF-BB induced 63 ± 6 % PDGFRα phosphorylated at Tyr^{754} and 31 ± 6 % PDGFRβ phosphorylated at Tyr^{1021} respectively to associate with NRP-1 [Figures 1C (iii and iv) and 1D (ii)]. These results are based on the proportion of receptor association within the immunoprecipitates. The values are likely to be indicative of total amounts of associated receptors, although the immunoprecipitation of each receptor from a cell lysate may not be 100 % efficient. Because the estimated proportions of total and phosphorylated PDGFRs which co-immunoprecipitated with NRP-1 in a particular cell lysate are comparable [see Figure 1D (i and ii)], the data suggest that virtually all of the PDGFRs which associate with NRP-1 are phosphorylated.

NRP-1 co-localized with phosphorylated PDGFRs

To further demonstrate that PDGF ligand stimulation induces NRP-1 to associate with PDGFRs, we examined the cellular distribution of NRP-1 and phosphorylated PDGFRs by immunofluorescence microscopy.

Analysis of unstimulated control MSCs demonstrated that PDGFRα-Tyr^{754} and PDGFRβ-Tyr^{1021} immunoreactivity predominantly localized around perinuclear regions, but was also detected at low levels peripherally, whereas NRP-1 immunoreactivity had a wider cellular distribution which in some cases extended towards the cell surface (Figures 2A and 2C). In contrast, MSCs exposed to PDGF-AA or PDGF-BB showed widespread cellular PDGFRα-Tyr^{754} (Figure 2B), or PDGFRβ-Tyr^{1021} (Figure 2D) immunoreactivity respectively. Co-localization analysis of unstimulated MSCs demonstrated minimal co-localization between NRP-1 and PDGFRα-Tyr^{754} and PDGFRβ-Tyr^{1021}; however, MSCs exposed to PDGF-AA or PDGF-BB resulted in a significant increase ($P < 0.001$, compared with unstimulated controls) in co-localization between NRP-1 and PDGFRα-Tyr^{754} or PDGFRβ-Tyr^{1021} respectively (Figure 2E), with PDGFRα-Tyr^{754} consistently producing the highest level of co-localization.

We also examined the cellular distribution of NRP-1 and total PDGFRs, using pan-PDGFR antibodies. In both unstimulated control and ligand-stimulated MSCs, while total PDGFRα immunoreactivity predominantly localized to perinuclear regions, the total PDGFRβ and NRP-1 immunoreactivity had a wider cellular distribution (Supplementary Figures S1A–S1D at http://www.BiochemJ.org/bj/427/bj4270029add.htm). Co-localization analysis demonstrated a low level of co-localization between NRP-1 and total PDGFRs in unstimulated MSCs, but a significant increase ($P < 0.001$, compared with unstimulated controls) on exposure to PDGF ligands (Supplementary Figure S1E), similar to the co-localization determined between NRP-1 and phosphorylated PDGFRs (Figure 2E), but at a relatively lower level.

To compare the distribution of ligand-stimulated NRP-1/PDGFR in MSCs with ligand-induced NRP-1/VEGFR2 co-localization in endothelial cells (HUVECs), we examined VEGF-A_{165}-induced NRP-1/PDGFRα-Tyr^{754} and NRP-1/PDGFRβ-Tyr^{1021} co-localization within MSCs, with VEGF-A_{165}-induced NRP-1/VEGFR2-Tyr^{1175} co-localization within HUVECs. Although HUVECs generally displayed a wider NRP-1 distribution than MSCs, unstimulated HUVECs and MSCs both demonstrated minimal NRP-1/VEGFR2 and NRP-1/PDGFR co-localization respectively (Figures 3A, 3C and 3E). In contrast, VEGF-A_{165} stimulation significantly increased ($P < 0.001$, compared with unstimulated controls) the co-localization of NRP-1 with VEGFR2-Tyr^{1175} in HUVECs (Figure 3B), as well as NRP-1 with PDGFRα-Tyr^{754} (Figure 3D) and PDGFRβ-Tyr^{1021} (Figure 3F) in MSCs.

Thus in MSCs, PDGF and VEGF-A_{165} ligands induce co-localization of NRP-1 with phosphorylated PDGFRs, similar to VEGF-A_{165}-induced NRP-1 co-localization with p-VEGFR2 in HUVECs.

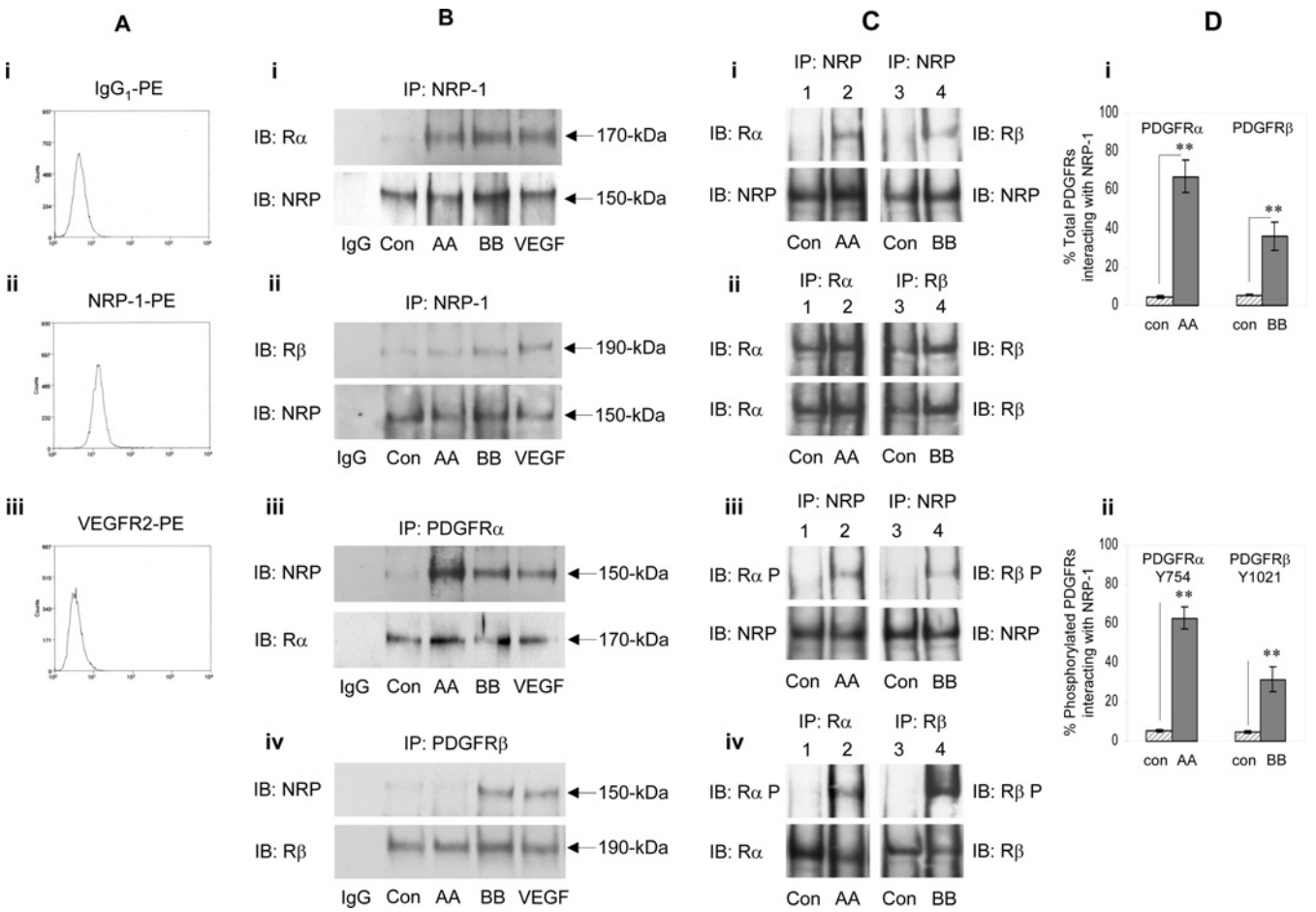

Figure 1 NRP-1 associated with phosphorylated PDGFRs

The association of NRP-1 with PDGFRs was evaluated. (**A**) Flow cytometry analysis of cell surface (i) IgG_1 used as a control, (ii) NRP-1 and (iii) VEGFR2. A representative example of three independent experiments is shown. (**B**) The association of NRP-1 with PDGFRs was examined by immunoprecipitation (IP) followed by immunoblot (IB) analysis. MSCs grown on gelatin and cultured for 24 h in serum-free conditions were unstimulated (Con) or stimulated with either 20 ng/ml PDGF-AA, PDGF-BB or VEGF-A_{165} for 10 min at 37 °C, then NRP-1 association with PDGFRs was determined by IP analysis of cell lysates. IP analysis using (i and ii) anti-NRP-1, (iii) anti-PDGFRα or (iv) anti-PDGFRβ, with anti-IgG_1 as a control, then NRP-1 association with PDGFRs detected by IB analysis using (i) anti-PDGFRα, (ii) anti-PDGFRβ or (iii and iv) anti-NRP-1, followed by IB analysis using anti-PDGFRs or NRP-1 as loading controls. A representative of three independent experiments is shown. (**C**) The percentage of (i and ii) total PDGFRs and (iii and iv) phosphorylated PDGFRs interacting with NRP-1 in a particular cell lysate was estimated by IP and IB analysis. Cell lysates were isolated from MSCs which were either unstimulated (Con) (lysates 1 and 3), or exposed to 20 ng/ml PDGF-AA (lysate 2) or PDGF-BB (lysate 4) for 10 min at 37 °C. Each cell lysate was then split into four separate 100 μg aliquots (i–iv) for IP analysis, using either anti-NRP-1, anti-PDGFRα (Rα) or anti-PDGFRβ (Rβ), then IB analysis using (i and ii) anti-PDGFRα or anti-PDGFRβ and (iii and iv) using anti-PDGFRα-Tyr^{754} or anti-PDGFRβ-Tyr^{1021}. As a loading control blots were re-probed using the corresponding IP antibody. The percentage of total PDGFRα or PDGFRβ interacting with NRP-1 was estimated by quantifying the IB analysis in (i) relative to the corresponding IB analysis in (ii), which was assumed to be 100 %. Similarly, the percentage of p-PDGFRα-Tyr^{754} or PDGFRβ-Tyr^{1021} interacting with NRP-1 was estimated by quantifying the IB analysis in (iii) relative to the corresponding IB analysis in (iv), which was taken to be 100 %. This approach gives the proportion of receptor association within the immunoprecipitates, but does not report the total amounts of receptors since the efficiency of each antibody in immunoprecipitating their receptor from a cell lysate may not be 100 %. (**D**) Histograms representing the co-immunoprecipitation data, showing the percentage of (i) total PDGFRα or PDGFRβ and (ii) p-PDGFRα-Tyr^{754} or PDGFRβ-Tyr^{1021}, which interacted with NRP-1. Values are mean percentage values $\pm$ S.D. determined from two independent experiments. $^{**}P < 0.001$, compared with unstimulated control.

NRP-1 regulated ligand-induced PDGFR phosphorylation

Having established that NRP-1 can associate and co-localize with phosphorylated PDGFRα and PDGFRβ, we investigated whether NRP-1 regulates PDGFR signalling. Following NRP-1 knockdown using two different siRNAs, NRP-1 protein expression was virtually ablated (Figure 4A), whereas RT–PCR analysis of their targeting specificity demonstrated they did not affect PDGFR transcripts (Figure 4B). We therefore utilized NRP-1 knockdown during the present study, first examining PDGFRα phosphorylation levels in serum-free conditions, using an ELISA for PDGFRα-Tyr^{742}. NRP-1 knockdown had little impact on basal levels of unstimulated PDGFRα phosphorylation (Figure 4C). However, exposure to PDGF-AA strongly stimulated PDGFRα phosphorylation, with NRP-1 knockdown dramatically reducing this phosphorylation to near-basal levels (Figure 4C). Although PDGF-CC and VEGF-A_{165} stimulated lower levels of PDGFRα phosphorylation, NRP-1 knockdown also reduced their phosphorylation to near-basal levels (Figure 4C). Thus NRP-1 markedly regulates PDGFRα signalling when stimulated by these growth factors. However, NRP-1 knockdown did not inhibit PDGF-AB-stimulated PDGFRα phosphorylation. The differential effects of NRP-1 knockdown on PDGF-CC- and PDGF-AB-induced PDGFRα phosphorylation reflect these growth-factor-binding specificities; PDGF-CC can bind the PDGFR$\alpha\alpha$ homodimer and PDGFR$\alpha\beta$ heterodimer [35,46],

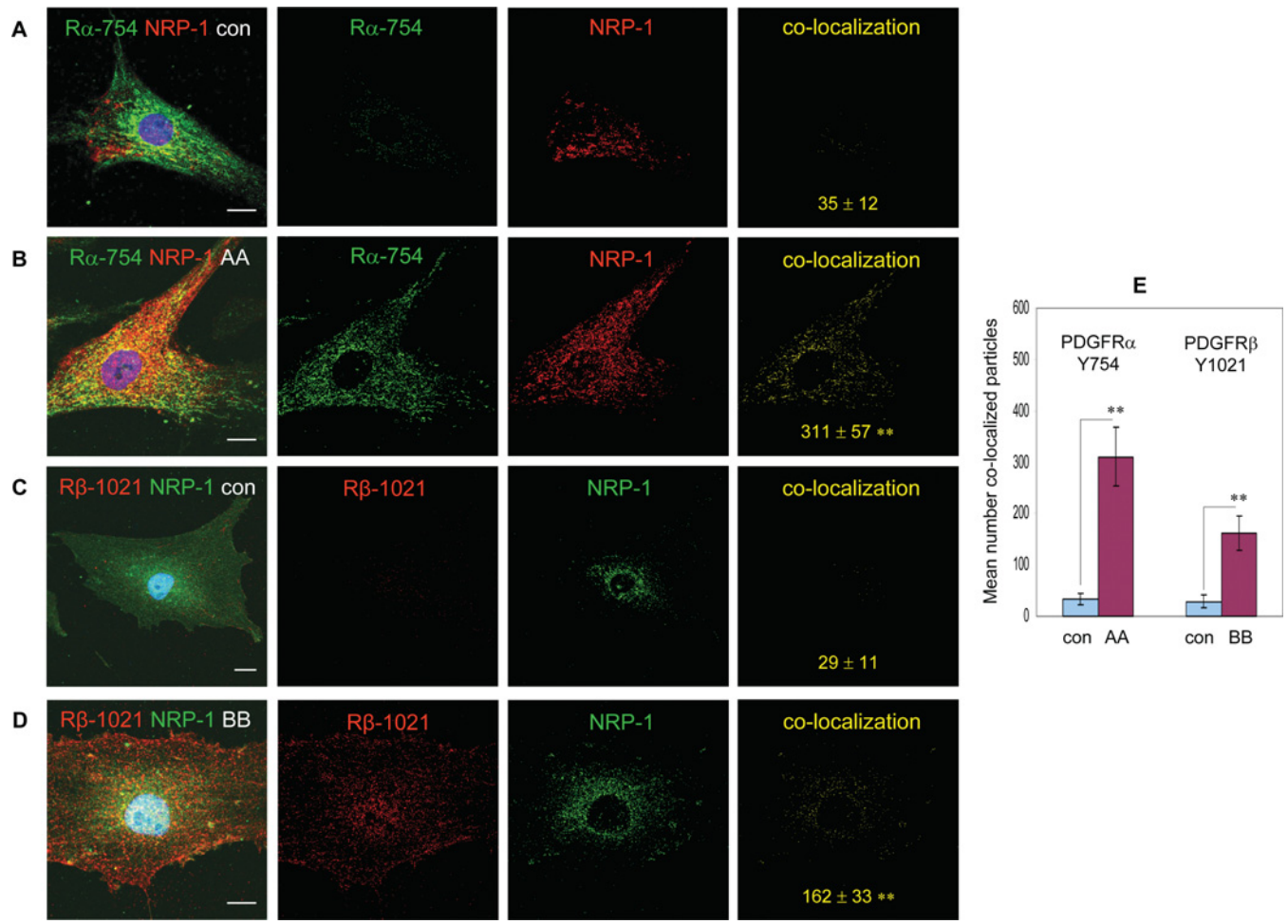

Figure 2 NRP-1 co-localized with phosphorylated PDGFRs

The cellular distribution of NRP-1 and phosphorylated PDGFRs was examined following ligand exposure. MSCs grown on 0.1 % gelatin were cultured for 24 h in serum-free conditions, exposed to PDGF ligands, then co-localization of NRP-1 with either phosphorylated PDGFRα at site Tyr^{754} or PDGFRβ at site Tyr^{1021} was examined by immunofluorescence microscopy. (**A**) Control unstimulated and (**B**) exposed to 20 ng/ml PDGF-AA for 10 min, showing PDGFRα-Tyr^{754} (green) and NRP-1 (red). (**C**) Control unstimulated and (**D**) exposed to 20 ng/ml PDGF-BB for 10 min, showing PDGFRβ-Tyr^{1021} (red) and NRP-1 (green). For each image, the corresponding red and green channels having similar threshold values and the same particle size range are shown, together with their co-localization represented by the image in yellow. The mean number of co-localized particles $\pm$ S.D. derived from six different single cell images is denoted in yellow. Nuclei are counter-stained with DAPI (blue). Representative images of at least four independent experiments are shown. Scale bars = 20 μm. (**E**) Histogram showing the ligand-induced increase in co-localization between NRP-1 and PDGFRα-Tyr^{754} or PDGFRβ-Tyr^{1021}, as determined by immunofluorescence analysis. Values are the mean number of co-localized particles $\pm$ S.D. derived from six different single cell images. $^{**}P < 0.001$, compared with the corresponding unstimulated control.

whereas PDGF-AB mainly binds PDGFR$\alpha\beta$ [36]. These results thus imply ligand-induced NRP-1-dependent PDGFRα homodimer signalling.

We also investigated whether NRP-1 regulates PDGFRβ signalling in serum-free conditions using an ELISA for PDGFRβ-Tyr^{751}. Control scrambled and target NRP-1 siRNA knockdowns resulted in comparable basal levels of unstimulated PDGFRβ phosphorylation (Figure 4D). While exposure to PDGF-BB strongly stimulated PDGFRβ phosphorylation, NRP-1 knockdown only partially reduced this phosphorylation (Figure 4D). However, whereas VEGF-A$_{165}$ stimulated lower levels of PDGFRβ phosphorylation, NRP-1 knockdown effectively inhibited this phosphorylation. Thus NRP-1 also regulates ligand-induced PDGFRβ phosphorylation. Since NRP-1 knockdown only decreased PDGF-BB-induced PDGFRβ phosphorylation by $\sim 44 \pm 5$ %, we examined whether NRP-1 knockdown primarily affects PDGF-BB-induced PDGFR$\alpha\beta$ phosphorylation, using PDGF-AB and PDGF-CC which bind the PDGFR$\alpha\beta$ heterodimer, but not a PDGFR$\beta\beta$ homodimer [35,36,46]. While both of these ligands induced PDGFRβ phosphorylation, indicating heterodimer stimulation, NRP-1 knockdown had no inhibitory effect in either case (Figure 4D). These results thus imply that NRP-1 influences ligand-induced PDGFRβ homodimer signalling.

NRP-1 regulated PDGFR-induced MSC migration and proliferation

Having established that NRP-1 plays a prominent role in regulating ligand-induced PDGFR signalling, the functional importance of this receptor cross-talk was investigated. We have previously demonstrated that VEGF-A- or PDGF-induced PDGFR signalling stimulates migration of MSCs [2]. In the present study we examined, in serum-free conditions, whether NRP-1 regulates PDGFR-mediated MSC migration. In the absence of ligand, control scrambled and target NRP-1 siRNA knockdowns resulted in comparable basal levels of unstimulated MSC migration (Figures 5A and 5B), similar to NRP-1 effects on PDGFR phosphorylation (Figures 4C and 4D). Exposure

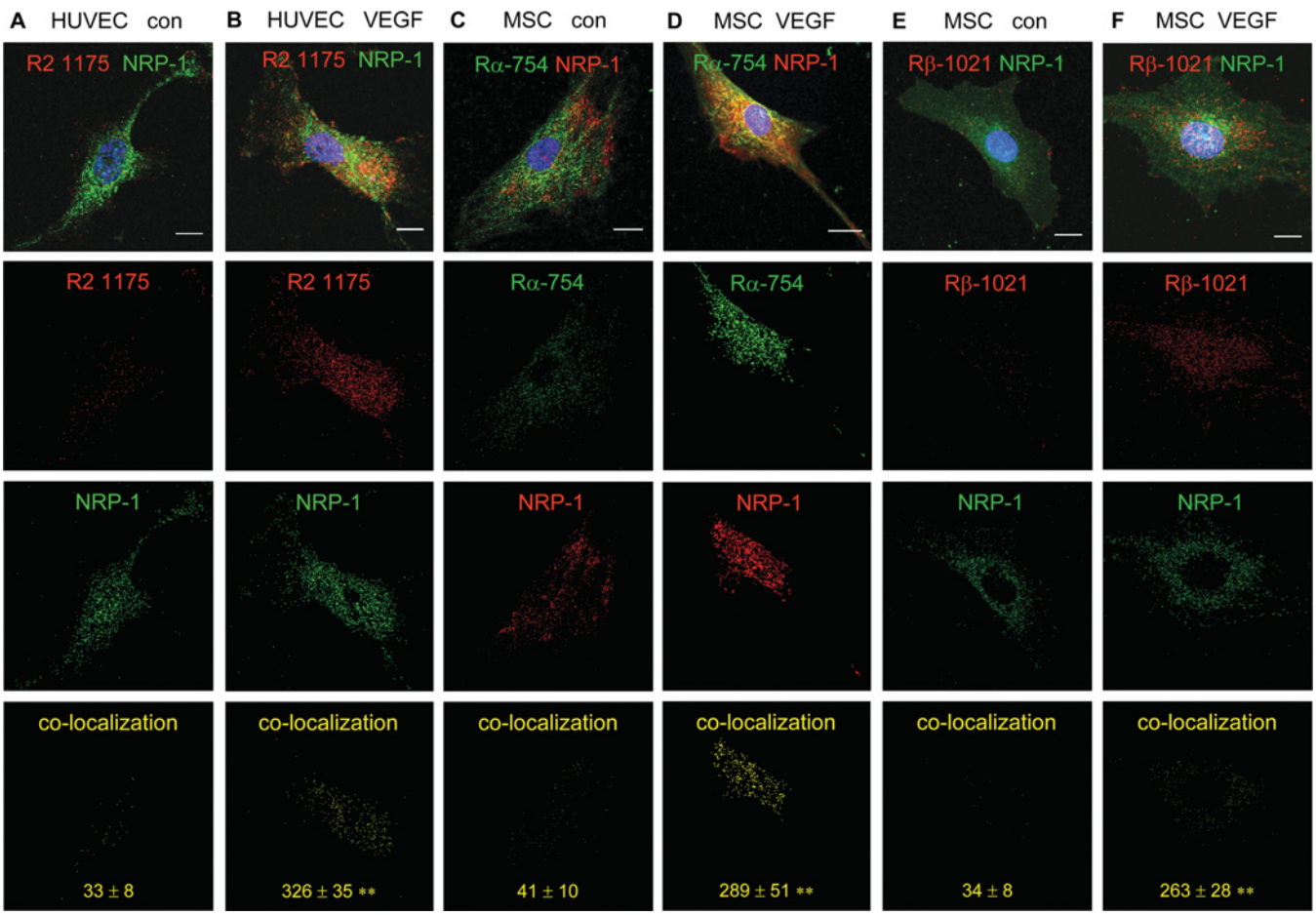

Figure 3 Comparison of VEGF-A-stimulated MSCs and HUVECs

The cellular distribution of NRP-1 was examined in MSCs and compared with HUVECs following VEGF-A_{165} stimulation. MSCs grown on 0.1 % gelatin were cultured for 24 h in serum-free conditions, then co-localization of NRP-1 with either PDGFRα phosphorylated at site Tyr^{754}, or PDGFRβ phosphorylated at site Tyr^{1021}, was examined by immunofluorescence microscopy. As a comparison, HUVECs grown on 0.1 % gelatin were cultured for 4 h in serum-free conditions, then co-localization of NRP-1 with VEGFR2 phosphorylated at site Tyr^{1175} was similarly determined. (**A**) Control unstimulated HUVEC and (**B**) HUVEC exposed to VEGF-A_{165} for 10 min, showing VEGFR2-Tyr^{1175} (red) and NRP-1 (green). (**C**) Control unstimulated MSC and (**D**) MSC exposed to VEGF-A_{165} for 10 min, showing PDGFRα-Tyr^{754} (green) and NRP-1 (red). (**E**) Control unstimulated MSC and (**F**) MSC exposed to 20 ng/ml VEGF-A_{165} for 10 min, showing PDGFRβ-Tyr^{1021} (red) and NRP-1 (green). Below each image, the corresponding red and green channels which have similar threshold values and the same particle size range are shown, together with their co-localization represented by the image in yellow. The mean number of co-localized particles $\pm$ S.D. derived from four different single cell images is denoted in yellow. $^{**}P < 0.001$, compared with the corresponding unstimulated control. Nuclei are counter-stained with DAPI (blue). Representative images of at least three independent experiments are shown. Scale bars = 20 μm.

to PDGF-AA (PDGFRα homodimer mediated) increased MSC migration, but was inhibited to virtually basal levels by NRP-1 knockdown (Figures 5A and 5B). Likewise, NRP-1 knockdown also decreased PDGF-BB- and VEGF-A_{165}-induced MSC migration, by $\sim 38 \pm 6$ % and $\sim 56 \pm 8$ % respectively (Figures 5A and 5B). Control scrambled and NRP-1 knockdowns, in the presence or absence of a VEGFR2 tyrosine kinase inhibitor, produced a similar level of VEGF-A_{165}-induced MSC migration (Figure 5B), indicating that a VEGFR2–NRP-1 complex was not contributing to VEGF-A_{165}-stimulated MSC migration. NRP-1 had a minimal effect on PDGF-CC- or PDGF-AB-induced MSC migration, confirming that these ligands probably stimulate migration through PDGFR$\alpha\beta$, but independently of NRP-1 (results not shown).

We also investigated the effects of NRP-1 knockdown on serum-stimulated MSC proliferation, in the absence or presence of supplementary PDGFR ligands. In serum growth medium alone, scrambled knockdown control MSCs proliferated up to 5 days, which was increased by supplementary PDGF-AA (Figure 5C) or PDGF-BB (Figure 5D). In comparison, at each timepoint NRP-1 knockdown significantly inhibited serum-stimulated MSC proliferation (Figures 5C and 5D). Moreover, NRP-1 knockdown decreased serum- and PDGF-ligand-supplemented proliferation to comparable levels (Figures 5C and 5D), indicating that NRP-1 knockdown was inhibiting PDGF-ligand-stimulated MSC proliferation. Similar results were obtained following NRP-1 knockdown of serum-stimulated MSC proliferation, in the absence or presence of supplementary VEGF-A_{165} (results not shown).

These results highlight the crucial contribution of NRP-1 to ligand-induced PDGFR-mediated MSC migration and proliferation.

NRP-1 regulated the assembly of MSC networks in Matrigel™

MSCs are critical contributors to neovascularization [47], and NRP-1 and PDGFRs play essential roles in this process [11,41]. Having established that NRP-1 plays a crucial role in regulating PDGFR-mediated MSC phosphorylation, migration

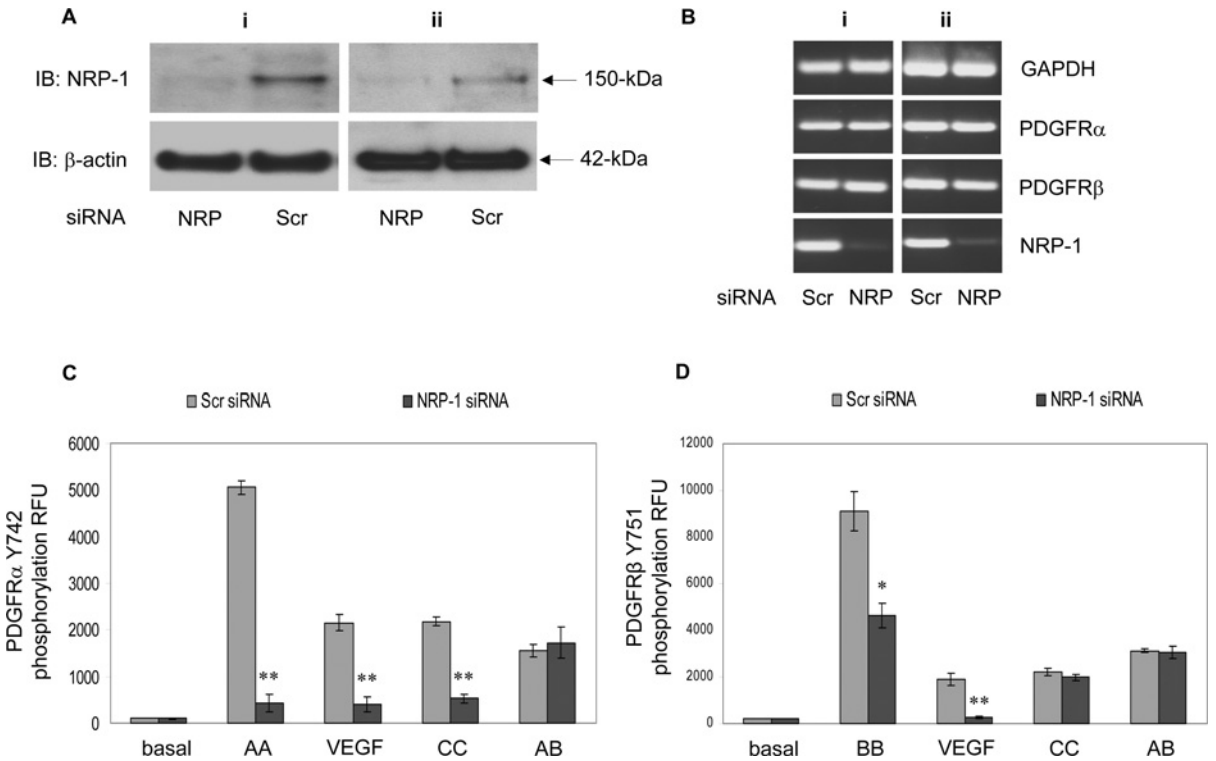

Figure 4 NRP-1 enhanced PDGFR phosphorylation

The effects of NRP-1 knockdown on PDGFR phosphorylation were determined. (**A**) Lysates from MSCs transfected with two different NRP-1 siRNAs, (i) (from Qiagen) and (ii) (from Ambion), or scrambled (Scr) control, were analysed for NRP-1 protein expression by immunoblot (IB) analysis using an anti-NRP-1 antibody. Membranes were reprobed with anti-β-actin as a loading control. (**B**) The targeting specificity of each siRNA knockdown was evaluated by RT–PCR analysis. Following siRNA knockdown using Scr control or two different NRP-1 siRNAs, (i) (from Qiagen) and (ii) (from Ambion), transcript expression for PDGFRα, PDGFRβ, NRP-1 and GAPDH (glyceraldehyde-3-phosphate dehydrogenase) as a control were determined. A representative of two independent experiments are shown. (**C** and **D**) Following siRNA knockdown with either Scr control or target NRP-1 siRNAs, MSCs in serum-free medium were exposed to either 50 ng/ml PDGF-AA, PDGF-BB, PDGF-AB, PDGF-CC or VEGF-A_{165}, or no growth factors (basal), for 10 min at 37 °C, then specific PDGFR tyrosine phosphorylation determined by cell-based ELISAs for (**C**) PDGFRα-Tyr^{742} or (**D**) PDGFRβ-Tyr^{751}. Tyrosine phosphorylation is represented by RFUs (relative fluorescent units). Values are mean normalized RFUs $\pm$ S.D. determined from two independent experiments performed in triplicate, using two different NRP-1 siRNAs. $^{**}P < 0.001$, $^{*}P < 0.005$, compared with the Scr siRNA control.

and proliferation, we went on to examine the function of NRP-1 in regulating the assembly of MSC network formation in a Matrigel™ culture model over 24 h.

We first evaluated the distribution of NRP-1 and p-PDGFRs during MSC network assembly by determining the immunolocalization of NRP-1 and PDGFRα-Tyr^{754} or PDGFRβ-Tyr^{1021}. During the initial stages of network assembly, MSCs exhibited intense widespread NRP-1 immunoreactivity (Figure 6). After 2 h seeding on to Matrigel™, high levels of PDGFRα-Tyr^{754} immunoreactivity were predominantly localized around the cell surface, where it conspicuously co-localized with NRP-1 (Figure 6A). In comparison, PDGFRβ-Tyr^{1021} was distributed throughout the cell, including the cell surface, but co-localization with NRP-1 was at a lower level (Figure 6B). After 6 h, PDGFRα-Tyr^{754} and NRP-1 co-localization had a wider cellular distribution (Figure 6C), whereas co-localization of PDGFRβ-Tyr^{1021} with NRP-1 became more prominent, especially at the cell surface (Figure 6D). By 24 h, MSCs had assembled to form abundant capillary-like network structures, which displayed high levels of co-localized NRP-1 with PDGFRα-Tyr^{754} and PDGFRβ-Tyr^{1021} (Figures 6E and 6F). To further substantiate these data, NRP-1 was also shown to co-localize with PDGFRα-Tyr^{720} and PDGFRβ-Tyr^{751} in MSC networks (Supplementary Figures S2A and S2B at http://www.BiochemJ.org/bj/427/bj4270029add.htm).

We confirmed that VEGFR2-Tyr^{1175} was not expressed in MSC networks (Supplementary Figure S3A at http://www.BiochemJ.org/bj/427/bj4270029add.htm). However, HUVECs in Matrigel™ readily formed capillary-like network structures, as expected, which not only displayed prominent co-localization of NRP-1 with VEGFR2-Tyr^{1175} (Supplementary Figure S3B), but also with PDGFRα-Tyr^{754} and PDGFRβ-Tyr^{1021} (Supplementary Figures S3C and S3D), suggesting that PDGFRs may also influence NRP-1 function in endothelial cells.

Having demonstrated that NRP-1 regulates PDGFR signalling and that both receptors are abundantly co-localized within MSC network structures, we went on to examine MSC network assembly following NRP-1 knockdown (Figure 7). Control scrambled siRNAs resulted in MSCs forming widespread capillary-like network structures within 24 h, containing pronounced NRP-1, PDGFRα-Tyr^{754} and PDGFRβ-Tyr^{1021} immunoreactivity and co-localization (Figures 7A, 7C and 7E), comparable with untransfected MSCs (see Figures 6E and 6F). However, after 24 h, NRP-1 knockdown MSCs produced distinctly disorganized structures (Figures 7B, 7D and 7F), containing significantly fewer branch points compared with control MSCs (Figure 7G). As expected, there was a dramatic reduction in NRP-1 immunoreactivity, confirming the efficiency of the knockdown, concurrent with a distinct decrease in both PDGFRα-Tyr^{754} and PDGFRβ-Tyr^{1021} immunoreactivity (Figures 7B and 7D).

These results indicate that NRP-1 regulation of PDGFR signalling plays a crucial role in directing MSC network assembly.

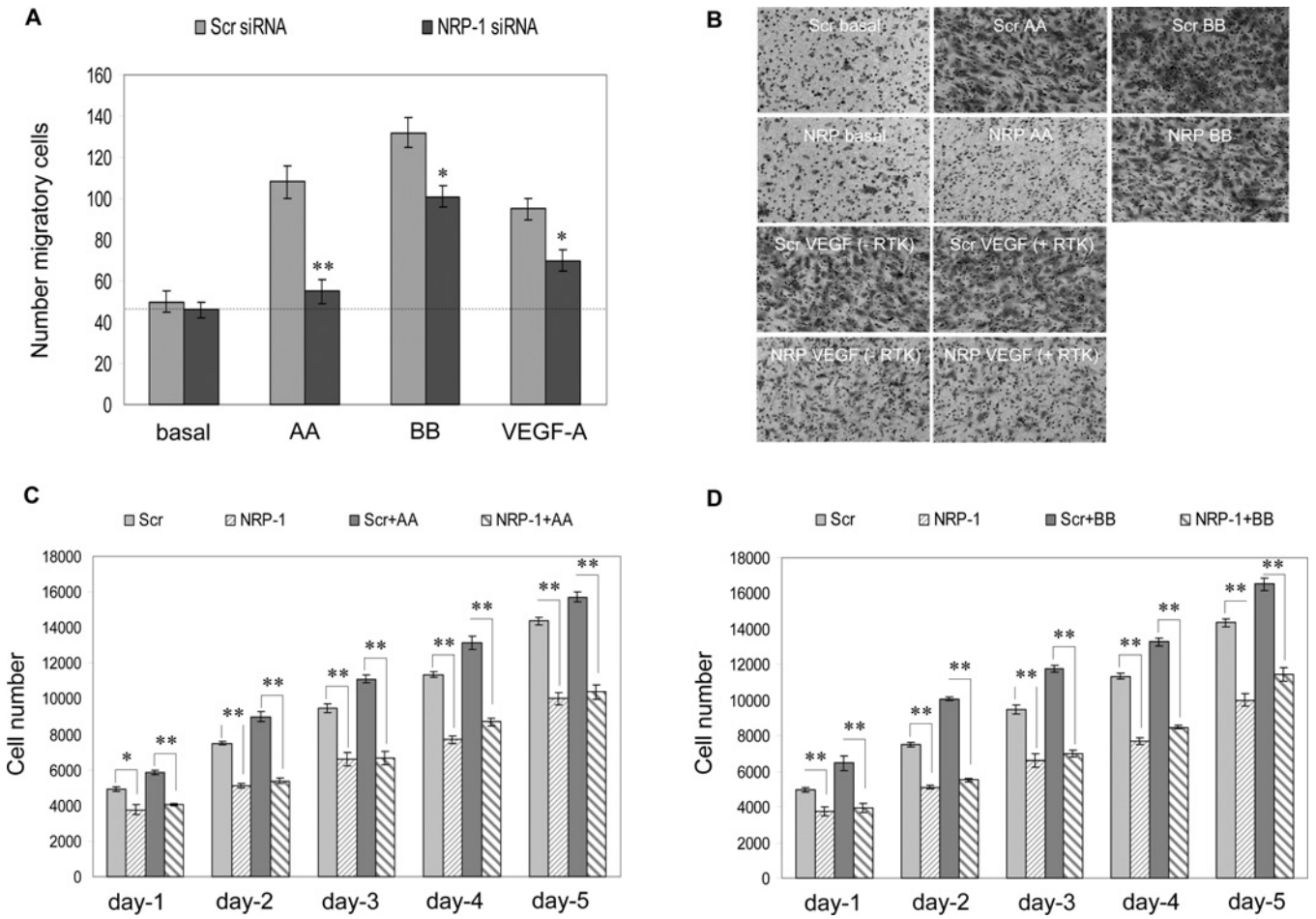

Figure 5 NRP-1 regulated PDGFR-mediated MSC migration and proliferation

The effects of NRP-1 knockdown on PDGFR-mediated migration and proliferation were investigated. (**A**) Following siRNA knockdown with either scrambled (Scr) control or target NRP-1 siRNAs, the effects on PDGFR-mediated migration were determined by exposing MSCs to 20 ng/ml PDGF-AA, PDGF-BB or VEGF-A_{165} in the lower half of a Boyden chamber for 5 h. The broken line represents the level of unstimulated MSC migration. Values are the mean number of migratory cells $\pm$ S.D. determined from ten random fields from each of three independent experiments. $^{**}P < 0.001$, $^{*}P < 0.005$, compared with the Scr siRNA control. (**B**) Representative images of migratory cells/field (using a 10$\times$ objective lens) on the membrane underside of a Boyden chamber after 5 h. Basal denotes unstimulated MSC migration. Ligand-stimulated MSC migration induced by 20 ng/ml PDGF-AA (AA), PDGF-BB (BB) or VEGF-A_{165} (VEGF) in the absence ($-$) or presence ($+$) of 100 nM VEGFR2 tyrosine kinase inhibitor (RTK). (**C** and **D**) Following siRNA knockdown with either Scr control or target NRP-1 siRNAs, the effects on PDGFR-mediated proliferation were determined by culturing MSCs for 5 days in either growth medium alone, or growth medium supplemented with (**C**) 10 ng/ml PDGF-AA or (**D**) 10 ng/ml PDGF-BB. Values are the mean cell number $\pm$ S.D. determined from triplicate assays from each of two independent experiments, using two different NRP-1 siRNAs. $^{**}P < 0.001$, $^{*}P < 0.005$, compared with the respective Scr siRNA control MSC proliferation.

NRP-1 regulated the assembly of MSC networks in a CAM model

To further demonstrate the importance of NRP-1 during MSC network formation, we examined the effects of NRP-1 knockdown utilizing an *in vivo* angiogenesis model system: the CAM of the developing chicken embryo [48]. Control scrambled or NRP-1 knockdown MSCs were seeded on to Matrigel™, then implanted in contact with a highly vascularized area of CAM for 24 h. As a control, identically prepared MSCs were also cultured *in vitro*. Following intimate association with the underlying CAM blood vessel microenvironment for 24 h, control MSCs formed widespread capillary-like network structures, containing abundant NRP-1, PDGFRα-Tyr^{754} and PDGFRβ-Tyr^{1021} immunoreactivity (Figures 8A, 8C, 8E and 8F). Both PDGFRα-Tyr^{754} and PDGFRβ-Tyr^{1021} displayed a high level of co-localization with NRP-1 in these *in vivo* assembled networks (Figures 8E and 8F), similar to the control *in-vitro*-cultured MSCs (results not shown) as previously demonstrated (see Figures 7A and 7C). In striking contrast, however, after 24 h of CAM exposure, NRP-1 knockdown resulted in widespread clusters of MSCs maintaining a rounded cellular morphology, which only exhibited trace levels of NRP-1, PDGFRα-Tyr^{754} or PDGFRβ-Tyr^{1021} immunoreactivity (Figures 8B and 8D). In comparison, the control *in-vitro*-cultured NRP-1 knockdown MSCs produced highly disorganized network assemblies (results not shown), as previously demonstrated (see Figures 7B and 7D).

Thus NRP-1 is critical for PDGFR signalling and the *in vivo* assembly of MSC network structures within the CAM vasculature microenvironment.

DISCUSSION

MSCs, which offer immense potential for cell-based tissue regeneration, have the capability to differentiate along vascular cell lineages [1–3]. Previously, we have shown that multipotent human MSCs express NRP-1 and PDGFRs, but not VEGFRs, and that PDGFs regulate MSC proliferation and migration, and the smooth muscle-specific cytoskeleton [2,4]. PDGFRα is an

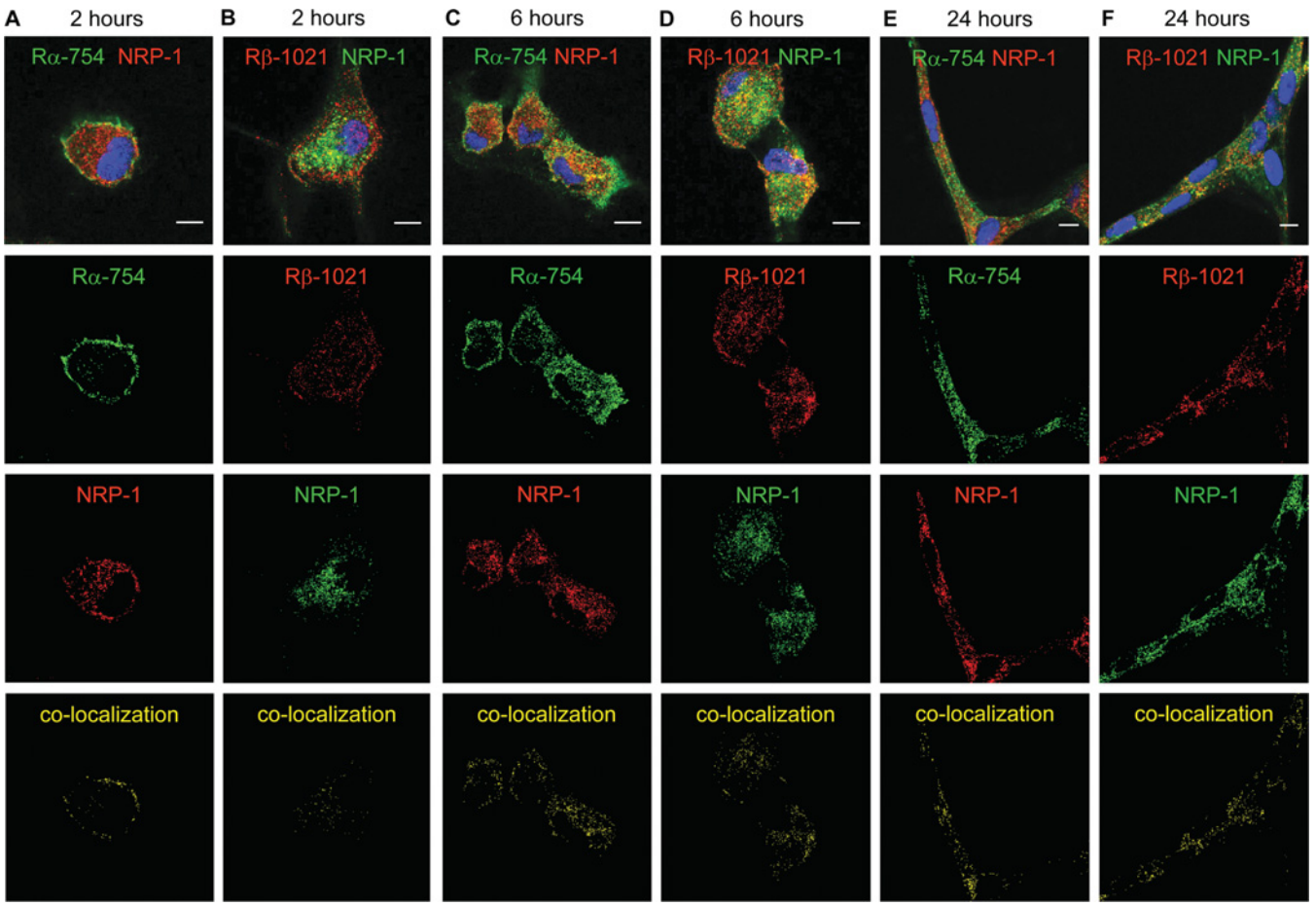

Figure 6 NRP-1 co-localization with PDGFRs during MSC network assembly

The co-localization of NRP-1 and PDGFRs was examined during the assembly of MSC networks. MSCs were seeded on to Matrigel™, then co-localization of NRP-1 with either PDGFRα phosphorylated at site Tyr^{754}, or PDGFRβ phosphorylated at site Tyr^{1021}, examined by immunofluorescence microscopy. MSCs cultured for (**A**) 2 h, (**C**) 6 h or (**E**) 24 h showing PDGFRα-Tyr^{754} (green) and NRP-1 (red). MSCs cultured for (**B**) 2 h, (**D**) 6 h or (**F**) 24 h showing PDGFRβ-Tyr^{1021} (red) and NRP-1 (green). Below each image, the corresponding red and green channels which have similar threshold values and the same particle size range are shown, together with their co-localization represented by the image in yellow. Nuclei are counter-stained with DAPI (blue). Representative images of at least four independent experiments are shown. Scale bars = 20 μm.

essential regulator of mesenchymal tissue formation in early embryonic development [38], and both PDGFRs contribute to vessel-wall development and remodelling following injury [42]. The essential contribution of NRP-1 to vascular development and neovascularization is also well documented [11] and, although its mechanisms of action remain incompletely understood, it is thought to regulate cell-surface-receptor clustering and signalling in a ligand-dependent manner. Our discovery that NRP-1 regulates the phosphorylation and signalling responses of PDGFRs, especially PDGFRα, sheds important light on fundamental cellular mechanisms of tissue development and neovascularization.

NRP-1 co-immunoprecipitated and co-localized with p-PDGFRs, and this association was significantly increased in the presence of growth-factor ligands, indicating that the PDGFR cross-talk with NRP-1 that we have identified may occur through a receptor-bridging mechanism. Indeed, *in-vitro*-binding studies indicate that PDGFRα and NRP-1 do not interact directly, but PDGF ligands, PDGF-AA, PDGF-BB and VEGF-A$_{165}$, all bind NRP-1 (Supplementary Figure S4 at http://www.BiochemJ.org/bj/427/bj4270029add.htm). PDGF-AA-mediated PDGFRα responses were particularly dependent upon NRP-1, implying that NRP-1 may be indispensable for PDGFRα function in tissue development and remodelling. PDGFRβ dependence on NRP-1 was also significant, so NRP-1 must regulate PDGFRβ-dependent smooth muscle cell migration, proliferation and differentiation during vessel-wall maturation and repair.

While NRP-1 is a transmembrane protein, immunofluorescence analysis demonstrated that the majority of NRP-1 in permeabilized MSCs and HUVECs was localized intracellularly. Exposure to VEGF-A$_{165}$ has been shown to promote NRP-1 on the surface of HUVECs to internalize, with immunofluorescence analysis of the permeablized HUVECs demonstrating NRP-1 predominantly localized around perinuclear regions [49]. Thus a similar mechanism resulting in rapid ligand-induced NRP-1 internalization may occur in MSCs.

MSCs readily formed extensive networks in Matrigel™ and CAM assays, highlighting their potential to contribute to blood-vessel formation. Co-localization of NRP-1 with phosphorylated PDGFRs occurred prominently in these networks, and the essential role for NRP-1/PDGFR cross-talk in network

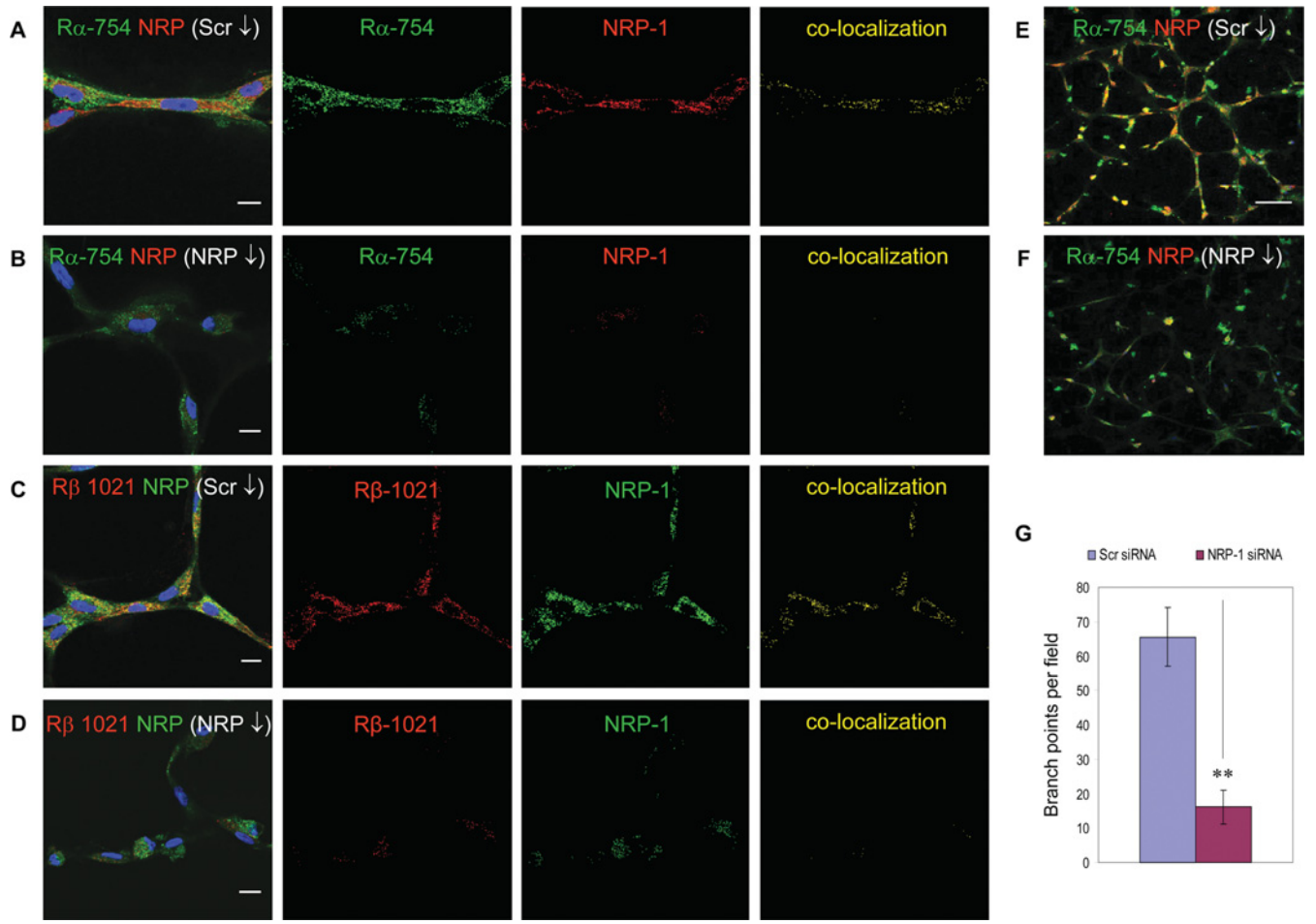

Figure 7 NRP-1 regulated MSC network assembly

The role of NRP-1 in regulating MSC network assembly was evaluated following NRP-1 knockdown. Following siRNA knockdown with either scrambled (Scr ↓) control or target NRP-1 (NRP ↓) siRNAs, MSCs were seeded on to Matrigel™ and cultured for 24 h, then co-localization of NRP-1 with either phosphorylated PDGFRα at site Tyr^{754} or PDGFRβ phosphorylated at site Tyr^{1021} was examined by immunofluorescence microscopy. Control knockdown MSCs, showing (**A**) PDGFRα-Tyr^{754} (green) and NRP-1 (red), and (**C**) PDGFRβ-Tyr^{1021} (red) and NRP-1 (green). NRP-1-knockdown MSCs, showing (**B**) PDGFRα-Tyr^{754} (green) and NRP-1 (red). (**D**) PDGFRβ-Tyr^{1021} (red) and NRP-1 (green). Nuclei are counter-stained with DAPI (blue). For each image, the corresponding red and green channels having similar threshold values and the same particle size range are shown, together with their co-localization represented by the image in yellow. Wider field images of control knockdown (**E**) and NRP-1-knockdown (**F**) MSCs showing PDGFRα-Tyr^{754} (green) and NRP-1 (red). Representative images of at least four independent experiments are shown. (**G**) Histogram representing the number of branch points per field at 24 h following Scr or target NRP-1 knockdown. Values are the mean number of branch points $\pm$ S.D. determined from at least six random fields from each of four independent experiments, $^{**}P < 0.001$, compared with the corresponding Scr siRNA control. Scale bars = 20 μm.

formation was confirmed by knockdown of NRP-1 which caused dramatically reduced PDGFR phosphorylation and grossly disrupted network formation. Prominent pericellular co-localization of NRP-1 with PDGFRα during early network formation suggests that this relationship is particularly important in initiating cellular changes leading to network formation. In MSCs, VEGF-A also induced NRP-1/PDGFR co-localization, similar to VEGF-A-induced NRP-1 co-localization with VEGFR2 in HUVECs. Since in HUVECs, NRP-1 co-localized with both VEGFR2 and PDGFRs in response to VEGF-A, NRP-1/PDGFR cross-talk is likely to contribute to endothelial functions mediated by VEGF-A. Our MSCs do not express VEGFRs, so their response to PDGFs and VEGF-A ligands is channelled through PDGFRs, but in endothelial and other cells expressing both VEGFRs and PDGFRs, the relative abundance of each receptor, local ligand concentrations and receptor affinities may combine to modify NRP-1-dependent receptor signals.

The essential contribution of PDGFRα to the formation of embryonic mesoderm and mesenchymal tissues is well documented [34], and we have demonstrated a high PDGFRα/PDGFRβ ratio in our MSCs [4]. PDGFRα-null mice die at around E10 (where E is embryonic day) due to vascular and other defects [40], whereas conditional null mice highlight that both PDGFRs are essential for early yolk sac vascular development [41]. The NRP-1-knockout mouse is also embryonic lethal, with major yolk sac and embryonic vascular defects, dying between E10 and E12.5 [50]. Thus the functional cross-talk between NRP-1 and both PDGFRs, especially PDGFRα, that we have identified, suggests a fundamental developmental relationship between these receptors.

In summary, in the present study we have shown ligand-dependent cross-talk between NRP-1 and phosphorylated PDGFRs that controls receptor signalling, migration, network formation and proliferation of MSCs. We have thus identified NRP-1 as an essential co-receptor for PDGFR signalling, which may critically contribute to the formation of blood vessels and other mesenchymal tissues. This mechanism may be exploited in the application of MSCs in tissue regeneration.

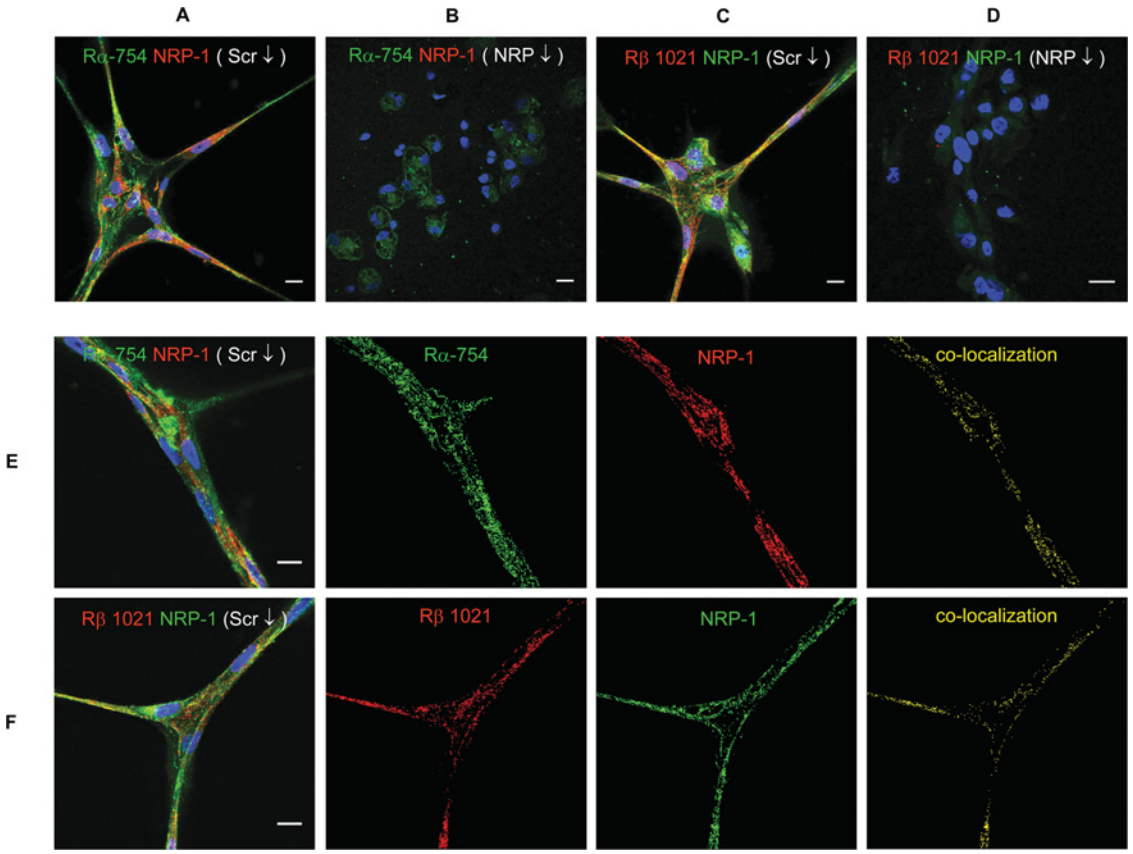

Figure 8 NRP-1 is essential for *in vivo* MSC networks

The effects of NRP-1 knockdown on MSC network formation was examined using an *in vivo* angiogenesis model system, the CAM of the developing chick embryo. Following siRNA knockdown with either Scrambled (Scr ↓) control or target NRP-1 (NRP ↓) siRNAs, MSCs were seeded on to Matrigel™ and implanted in direct contact with a highly vascularized area of CAM for 24 h, then co-localization of NRP-1 with either phosphorylated PDGFRα at site Tyr^{754} or PDGFRβ phosphorylated at site Tyr^{1021} was examined by immunofluorescence microscopy. Control knockdown MSCs, showing (**A**) PDGFRα-Tyr^{754} (green) and NRP-1 (red), (**C**) PDGFRβ-Tyr^{1021} (red) and NRP-1 (green). NRP-1-knockdown MSCs, showing (**B**) PDGFRα-Tyr^{754} (green) and NRP-1 (red), (**D**) PDGFRβ-Tyr^{1021} (red) and NRP-1 (green). Control knockdown MSCs, showing (**E**) PDGFRα-Tyr^{754} (green) and NRP-1 (red), (**F**) PDGFRβ-Tyr^{1021} (red) and NRP-1 (green). For each image, the corresponding red and green channels having similar threshold values and the same particle size range are shown, together with their co-localization represented by the image in yellow. Nuclei are counter-stained with DAPI (blue). Representative images of two independent experiments are shown. Scale bars = 20 μm.

AUTHOR CONTRIBUTION

Stephen Ball contributed to experimental design, conducted MSC experiments and contributed to the writing of the manuscript. Christopher Bayley conducted the molecular-binding studies shown in Supplementary Figure S4. Adrian Shuttleworth contributed to experimental design and the writing of the manuscript. Cay Kielty directed the experiments and contributed to the writing of the manuscript.

ACKNOWLEDGEMENTS

We thank Ms Jemima Whyte (University of Manchester, Manchester, U.K.) for her contribution towards developing the CAM assay, and Ms Maybo Chiu for recombinant VEGF-A used in the binding assays.

FUNDING

This work was funded by the Medical Research Council (UK) [grant number G0700712]. C.M.K. holds a Royal Society Wolfson Research Merit award.

REFERENCES

1 Oswald, J., Boxberger, S., Jorgensen, B., Feldmann, S., Ehninger, G., Bornhauser, M. and Werner, C. (2004) Mesenchymal stem cells can differentiate into endothelial cells *in vitro*. Stem Cells **22**, 377–384

2 Ball, S. G., Shuttleworth, C. A. and Kielty, C. M. (2007) Vascular endothelial growth factor can signal through platelet-derived growth factor receptors. J. Cell Biol. **177**, 489–500

3 Chen, M. Y., Lie, P. C., Li, Z. L. and Wei, X. (2009) Endothelial differentiation of Wharton's jelly-derived mesenchymal stem cells in comparison with bone marrow-derived mesenchymal stem cells. Exp. Hematol. **37**, 629–640

4 Ball, S. G., Shuttleworth, C. A. and Kielty, C. M. (2007) Platelet-derived growth factor receptor-α is a key determinant of smooth muscle α-actin in bone marrow-derived mesenchymal stem cells. Int. J. Biochem. Cell Biol. **39**, 379–391.

5 Chen, H., Chedotal, A., He, Z., Goodman, C. S. and Tessier-Lavigne, M. (1997) Neuropilin-2, a novel member of the neuropilin family, is a high affinity receptor for the semaphorins Sema E and Sema IV but not Sema III. Neuron **19**, 547–559

6 Kolodkin, A. L., Levengood, D. V., Rowe, E. G., Tai, Y. T., Giger, R. J. and Ginty, D. D. (1997) Neuropilin is a semaphorin III receptor. Cell **90**, 753–762

7 Soker, S., Takashima, S., Miao, H. Q., Neufeld, G. and Klagsbrun, M. (1998) Neuropilin-1 is expressed by endothelial and tumor cells as an isoform-specific receptor for vascular endothelial growth factor. Cell **92**, 735–745

8 Takahashi, T., Nakamura, F., Jin, Z., Kalb, R. G. and Strittmatter, S. M. (1998) Semaphorins A and E act as antagonists of neuropilin-1 and agonists of neuropilin-2 receptors. Nat. Neurosci. **1**, 487–493

9 Serini, G., Valdembri, D., Zanivan, S., Morterra, G., Burkhardt, C., Caccavari, F., Zammataro, L., Primo, L., Tamagnone, L., Logan, M. et al. (2003) Class 3 semaphorins control vascular morphogenesis by inhibiting integrin function. Nature **424**, 391–397

10 Gitler, A. D., Lu, M. M. and Epstein, J. A. (2004) PlexinD1 and semaphorin signaling are required in endothelial cells for cardiovascular development. Dev. Cell **7**, 107–116

11 Pellet-Many, C., Frankel, P., Jia, H. and Zachary, I. (2008) Neuropilins: structure, function and role in disease. Biochem. J. **411**, 211–216
12 Kitsukawa, T., Shimono, A., Kawakami, A., Kondoh, H. and Fujisawa, H. (1995) Overexpression of a membrane protein, neuropilin, in chimeric mice causes anomalies in the cardiovascular system, nervous system and limbs. Development **121**, 4309–4318
13 Kawasaki, T., Kitsukawa, T., Bekku, Y., Matsuda, Y., Sanbo, M., Yagi, T. and Fujisawa, H. (1999) A requirement for neuropilin-1 in embryonic vessel formation. Development **126**, 4895–902
14 Lee, P., Goishi, K., Davidson, A. J., Mannix, R., Zon, L. and Klagsbrun, M. (2002) Neuropilin-1 is required for vascular development and is a mediator of VEGF-dependent angiogenesis in zebrafish. Proc. Natl. Acad. Sci. U.S.A. **99**, 10470–10475
15 Cai, H. and Reed, R. R. (1999) Cloning and characterization of neuropilin-1-interacting protein: a PSD-95/Dlg/ZO-1 domain-containing protein that interacts with the cytoplasmic domain of neuropilin-1. J. Neurosci. **19**, 6519–6527
16 Wang, L., Mukhopadhyay, D. and Xu, X. (2006) C-terminus of RGS-GAIP-interacting protein conveys neuropilin-1-mediated signaling during angiogenesis. FASEB J. **20**, 1513–1515
17 Bielenberg, D. R., Pettaway, C. A., Takashima, S. and Klagsbrun, M. (2006) Neuropilins in neoplasms: expression, regulation, and function. Exp. Cell Res. **312**, 584–593
18 Guttmann-Raviv, N., Kessler, O., Shraga-Heled, N., Lange, T., Herzog, Y. and Neufeld, G. (2006) The neuropilins and their role in tumorigenesis and tumor progression. Cancer Lett. **231**, 1–11
19 Geretti, E., Shimizu, A. and Klagsbrun, M. (2008) Neuropilin structure governs VEGF and semaphorin binding and regulates angiogenesis. Angiogenesis **11**, 31–39
20 Pan, Q., Chathery, Y., Wu, Y., Rathore, N., Tong, R. K., Peale, F., Bagri, A., Tessier-Lavigne, M., Koch, A. W. and Watts, R. J. (2007) Neuropilin-1 binds to VEGF121 and regulates endothelial cell migration and sprouting. J. Biol. Chem. **282**, 24049–24056
21 Salikhova, A., Wang, L., Lanahan, A. A., Liu, M., Simons, M., Leenders, W. P., Mukhopadhyay, D. and Horowitz, A. (2008) Vascular endothelial growth factor and semaphorin induce neuropilin-1 endocytosis via separate pathways. Circ. Res. **103**, e71–e79
22 Whitaker, G. B., Limberg, B. J. and Rosenbaum, J. S. (2001) Vascular endothelial growth factor receptor-2 and neuropilin-1 form a receptor complex that is responsible for the differential signaling potency of VEGF(165) and VEGF(121). J. Biol. Chem. **276**, 25520–25531
23 Neufeld, G., Kessler, O. and and Herzog, Y. (2002) The interaction of Neuropilin-1 and Neuropilin-2 with tyrosine-kinase receptors for VEGF. Adv. Exp. Med. Biol. **515**, 81–90
24 Soker, S., Miao, H. Q., Nomi, M., Takashima, S. and Klagsbrun, M. (2002) VEGF165 mediates formation of complexes containing VEGFR-2 and neuropilin-1 that enhance VEGF165-receptor binding. J. Cell. Biochem. **85**, 357–368
25 Shraga-Heled, N., Kessler, O., Prahst, C., Kroll, J., Augustin, H. and Neufeld, G. (2007) Neuropilin-1 and neuropilin-2 enhance VEGF121 stimulated signal transduction by the VEGFR-2 receptor. FASEB J. **21**, 915–926
26 Kawamura, H., Li, X., Goishi, K., van Meeteren, L. A., Jakobsson, L., Cebe-Suarez, S., Shimizu, A., Edholm, D., Ballmer-Hofer, K., Kjellen, L. et al. (2008) Neuropilin-1 in regulation of VEGF-induced activation of p38MAPK and endothelial cell organization. Blood **112**, 3638–3649
27 Prahst, C., Heroult, M., Lanahan, A. A., Uziel, N., Kessler, O., Shraga-Heled, N., Simons, M., Neufeld, G. and Augustin, H. G. (2008) Neuropilin-1-VEGFR-2 complexing requires the PDZ-binding domain of neuropilin-1. J. Biol. Chem. **283**, 25110–25114
28 Bachelder, R. E., Crago, A., Chung, J., Wendt, M. A., Shaw, L. M., Robinson, G. and Mercurio, A. M. (2001) Vascular endothelial growth factor is an autocrine survival factor for neuropilin-expressing breast carcinoma cells. Cancer Res. **61**, 5736–5740
29 Bachelder, R. E., Wendt, M. A. and Mercurio, A. M. (2002) Vascular endothelial growth factor promotes breast carcinoma invasion in an autocrine manner by regulating the chemokine receptor CXCR4. Cancer Res. **62**, 7203–7206
30 West, D. C., Rees, C. G., Duchesne, L., Patey, S. J., Terry, C. J., Turnbull, J. E., Delehedde, M., Heegaard, C. W., Allain, F., Vanpouille, C. et al. (2005) Interactions of multiple heparin binding growth factors with neuropilin-1 and potentiation of the activity of fibroblast growth factor-2. J. Biol. Chem. **280**, 13457–13464
31 Sulpice, E., Plouet, J., Berge, M., Allanic, D., Tobelem, G. and Merkulova-Rainon, T. (2008) Neuropilin-1 and neuropilin-2 act as coreceptors, potentiating proangiogenic activity. Blood **111**, 2036–2045
32 Banerjee, S., Sengupta, K., Dhar, K., Mehta, S., D'Amore, P. A., Dhar, G. and Banerjee, S. K. (2006) Breast cancer cells secreted platelet-derived growth factor-induced motility of vascular smooth muscle cells is mediated through neuropilin-1. Mol. Carcinog. **45**, 871–880
33 Holmes, D. I. and Zachary, I. (2005) The vascular endothelial growth factor (VEGF) family: angiogenic factors in health and disease. Genome Biol. **6**, 209–219
34 Andrae, J., Gallini, R. and Betsholtz, C. (2008) Role of platelet-derived growth factors in physiology and medicine. Genes Dev. **22**, 1276–1312
35 Fredriksson, L., Li, H. and Eriksson, U. (2004) The PDGF family: four gene products form five dimeric isoforms. Cytokine Growth Factor Rev. **15**, 197–204
36 Zhang, J., Cao, R., Zhang, Y., Jia, T., Cao, Y. and Wahlberg, E. (2009) Differential roles of PDGFR-α and PDGFR-β in angiogenesis and vessel stability. FASEB J. **23**, 153–163
37 Palmieri, S. L., Payne, J., Stiles, C. D., Biggers, J. D. and Mercola, M. (1992) Expression of mouse PDGF-A and PDGF alpha-receptor genes during pre- and post-implantation development: evidence for a developmental shift from an autocrine to a paracrine mode of action. Mech. Dev. **39**, 181–191
38 Soriano, P. (1997) The PDGFα receptor is required for neural crest cell development and for normal patterning of the somites. Development **124**, 2691–2700
39 Darabi, R., Gehlbach, K., Bachoo, R. M., Kamath, S., Osawa, M., Kamm, K. E. and Perlingeiro, R. C. (2008) Functional skeletal muscle regeneration from differentiating embryonic stem cells. Nat. Med. **14**, 134–143
40 Bostrom, H., Willetts, K., Pekny, M., Leveen, P., Lindahl, P., Hedstrand, H., Pekna, M., Hellstrom, M., Gebre-Medhin, S., Schalling, M. et al. (1996) PDGF-A signaling is a critical event in lung alveolar myofibroblast development and alveogenesis. Cell **85**, 863–873
41 French, W. J., Creemers, E. E. and Tallquist, M. D. (2008) Platelet-derived growth factor receptors direct vascular development independent of vascular smooth muscle cell function. Mol. Cell. Biol. **28**, 5646–5657
42 Raines, E. W. (2004) PDGF and cardiovascular disease. Cytokine Growth Factor Rev. **15**, 237–254
43 Cimato, T., Beers, J., Ding, S., Ma, M., McCoy, J. P., Boehm, M. and Nabel, E. G. (2009) Neuropilin-1 identifies endothelial precursors in human and murine embryonic stem cells before CD34 expression. Circulation **119**, 2170–2178
44 Zacchigna, S., Pattarini, L., Zentilin, L., Moimas, S., Carrer, A., Sinigaglia, M., Arsic, N., Tafuro, S., Sinagra, G. and Giacca, M. J. (2008) Bone marrow cells recruited through the neuropilin-1 receptor promote arterial formation at the sites of adult neoangiogenesis in mice. J. Clin, Invest. **118**, 2062–2075
45 Ball, S. G., Shuttleworth, C. A. and Kielty, C. M. (2004) Direct cell contact influences bone marrow mesenchymal stem cell fate. Int. J. Biochem. Cell Biol. **36**, 714–727
46 Gilbertson, D. G., Duff, M. E., West, J. W., Kelly, J. D., Sheppard, P. O., Hofstrand, P. D., Gao, Z., Shoemaker, K., Bukowski, T. R., Moore, M. et al. (2001) Platelet-derived growth factor C (PDGF-C), a novel growth factor that binds to PDGF α and β receptor. J. Biol. Chem. **276**, 27406–27414
47 Silva, G. V., Litovsky, S., Assad, J. A., Sousa, A. L., Martin, B. J., Vela, D., Coulter, S. C., Lin, J., Ober, J., Vaughn, W. K. et al. (2005) Mesenchymal stem cells differentiate into an endothelial phenotype, enhance vascular density, and improve heart function in a canine chronic ischemia model. Circulation **111**, 150–156
48 Ribatti, D., Vacca, A., Roncali, L. and Dammacco, F. (1996) The chick embryo chorioallantoic membrane as a model for in vivo research on angiogenesis. Int. J. Dev. Biol. **40**, 1189–1197
49 Narazaki, M. and Tosato, G. (2006) Ligand-induced internalization selects use of common receptor neuropilin-1 by $VEGF_{165}$ and semaphorin3A. Blood **107**, 3892–3901
50 Takashima, S., Kitakaze, M., Asakura, M., Asanuma, H., Sanada, S., Tashiro, F., Niwa, H., Miyazaki Ji, J., Hirota, S., Kitamura, Y. et al. (2002) Targeting of both mouse neuropilin-1 and neuropilin-2 genes severely impairs developmental yolk sac and embryonic angiogenesis. Proc. Natl. Acad. Sci. U.S.A. **99**, 3657–3662

Received 30 September 2009/25 January 2010; accepted 26 January 2010
Published as BJ Immediate Publication 26 January 2010, doi:10.1042/BJ20091512

Biochem. J. (2010) **427**, 29–40 (Printed in Great Britain) doi:10.1042/BJ20091512

online data

SUPPLEMENTARY ONLINE DATA

Neuropilin-1 regulates platelet-derived growth factor receptor signalling in mesenchymal stem cells

Stephen G. BALL, Christopher BAYLEY, C. Adrian SHUTTLEWORTH and Cay M. KIELTY[1]

Wellcome Trust Centre for Cell-Matrix Research, Faculty of Life Sciences, University of Manchester, Manchester M13 9PT, U.K.

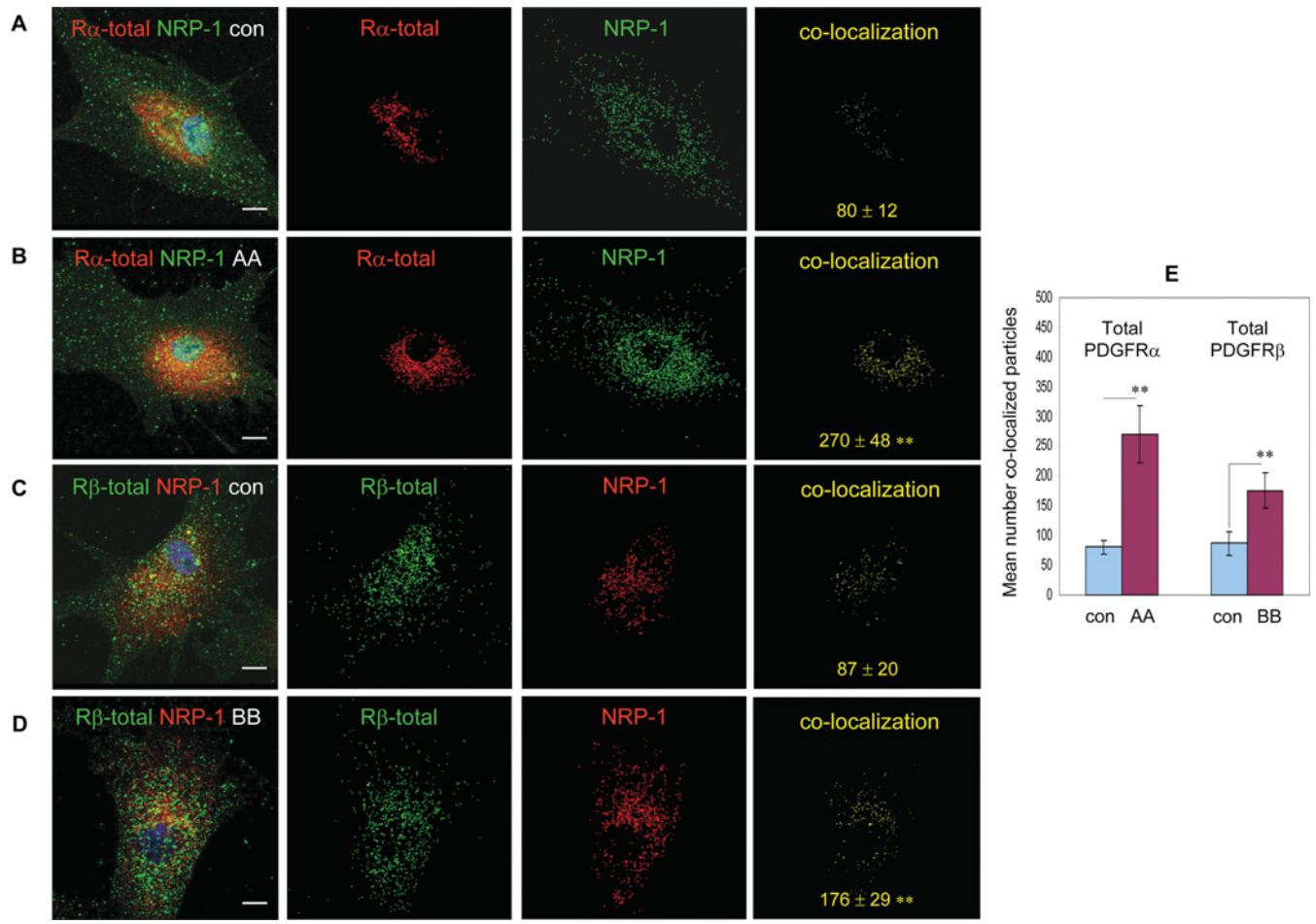

Figure S1 Co-localization of NRP-1 with total PDGFRs

The cellular distribution of NRP-1 and total PDGFRs was examined using pan-PDGFR antibodies. MSCs grown on 0.1% gelatin were cultured for 24 h in serum-free conditions, exposed to PDGF ligands, then co-localization of NRP-1 with either total PDGFRα or PDGFRβ was examined by immunofluorescence microscopy. (**A**) Control unstimulated and (**B**) exposed to 20 ng/ml PDGF-AA for 10 min, showing total PDGFRα (red) and NRP-1 (green). (**C**) Control unstimulated and (**D**) exposed to 20 ng/ml PDGF-BB for 10 min, showing total PDGFRβ (green) and NRP-1 (red). For each image, the corresponding red and green channels having similar threshold values and the same particle size range are shown, together with their co-localization represented by the image in yellow. The mean number of co-localized particles$\pm$S.D. derived from four different single-cell images is denoted in yellow. Nuclei are counter-stained with DAPI (blue). Representative images of at least six independent experiments are shown. Scale bars $=20$ μm. (**E**) Histogram showing the ligand-induced increase in co-localization between NRP-1 and total PDGFRα or PDGFRβ, as determined by immunofluorescence analysis. Values are the mean number of co-localized particles$\pm$S.D. derived from six different single-cell images. $^{**}P<0.001$, compared with the corresponding unstimulated control.

[1] To whom correspondence should be addressed (email cay.kielty@manchester.ac.uk).

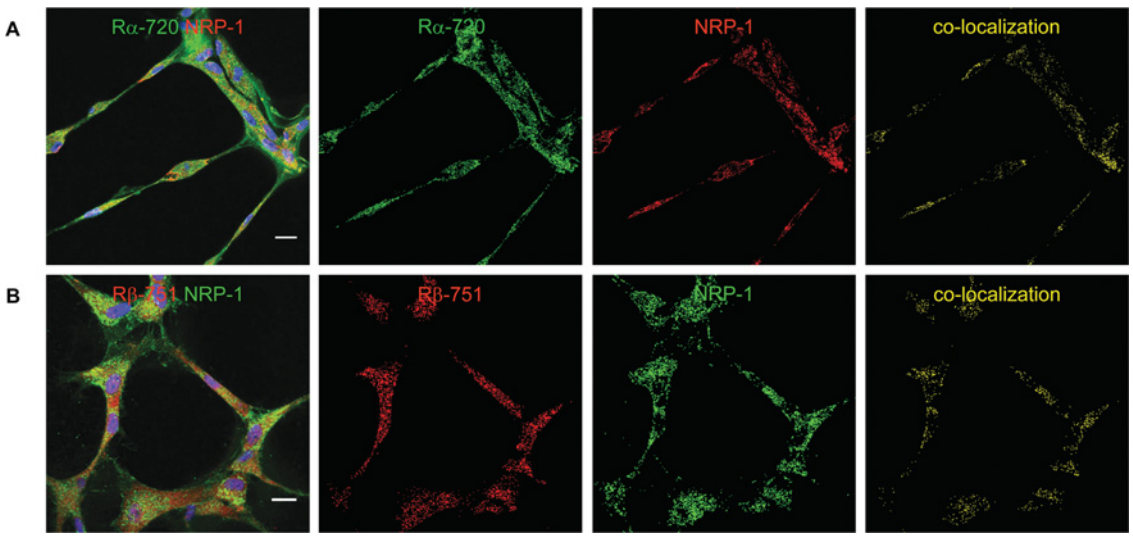

Figure S2 Co-localization of NRP-1 with additional phosphorylated PDGFR sites

The co-localization of NRP-1 with two additional PDGFR phosphorylation sites was examined during the assembly of MSC networks. MSCs were seeded on to Matrigel^{TM} and cultured for 24 h, then co-localization of NRP-1 with either PDGFRα at site Tyr^{720}, or PDGFRβ at site Tyr^{751} was examined by immunofluorescence microscopy. (**A**) MSCs showing PDGFRα-Tyr^{720} (green) and NRP-1 (red). (**B**) MSCs showing PDGFRβ-Tyr^{751} (red) and NRP-1 (green). For each image, the corresponding red and green channels which have similar threshold values and the same particle size range are shown, together with their co-localization represented by the image in yellow. Nuclei are counterstained with DAPI (blue). Representative images of at least four independent experiments are shown. Scale bars = 20 μm.

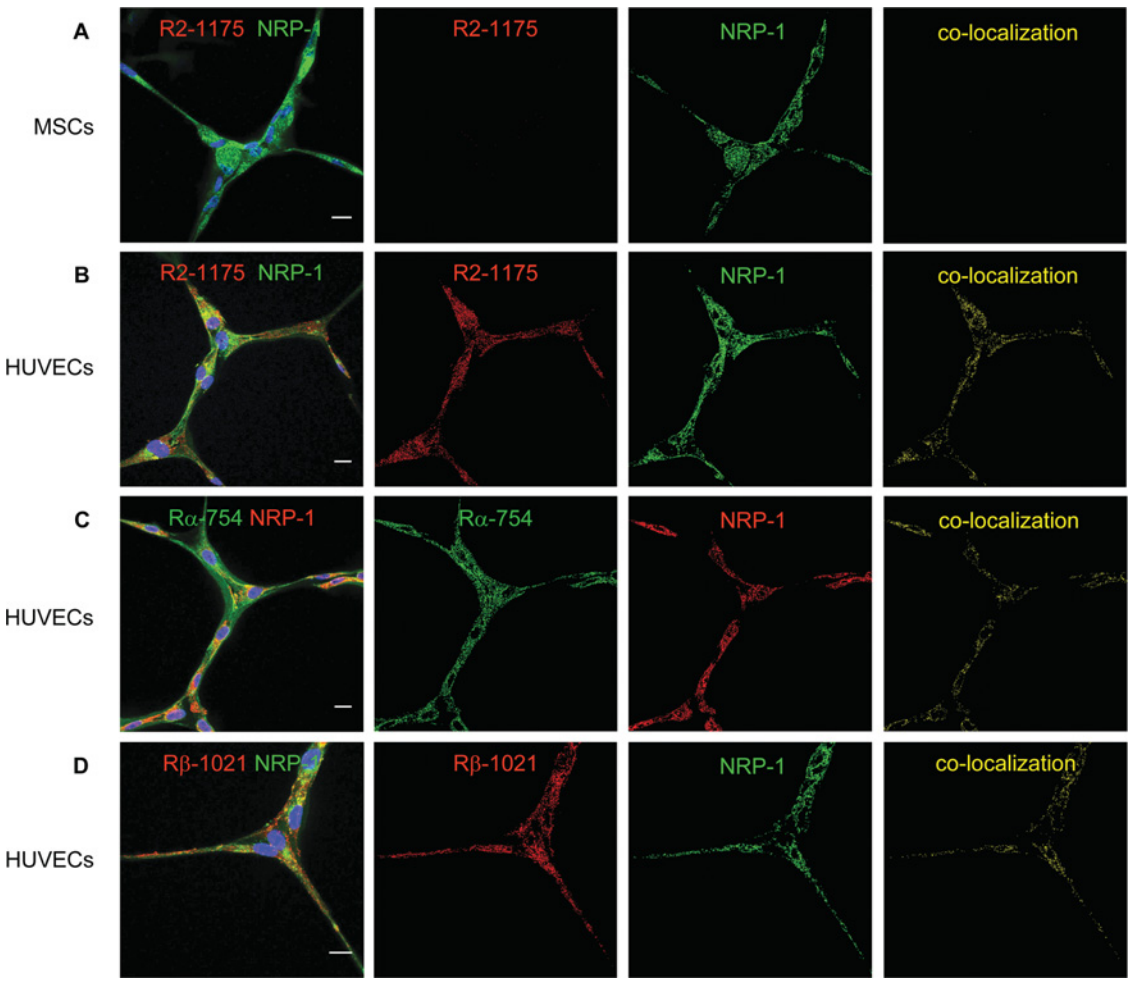

Figure S3 NRP-1 co-localization with PDGFRs in HUVEC networks

The co-localization of NRP-1 and PDGFRs was examined in HUVEC networks. HUVECs or MSCs were seeded on to Matrigel™ and cultured for 24 h, then co-localization of NRP-1 with either VEGFR2 at site Tyr^{1175}, PDGFRα at site Tyr^{754} or PDGFRβ at site Tyr^{1021}, was examined by immunofluorescence microscopy. (**A**) MSCs showing VEGFR2-Tyr^{1175} (red) and NRP-1 (green). (**B**) HUVECs showing VEGFR2-Tyr^{1175} (red) and NRP-1 (green). (**C**) HUVECs showing PDGFRα-Tyr^{754} (green) and NRP-1 (red). (**D**) HUVECs showing PDGFRβ-Tyr^{1021} (red) and NRP-1 (green). For each image, the corresponding red and green channels which have similar threshold values and the same particle size range are shown, together with their co-localization represented by the image in yellow. Nuclei are counterstained with DAPI (blue). Representative images of at least three independent experiments are shown. Scale bars = 20 μm.

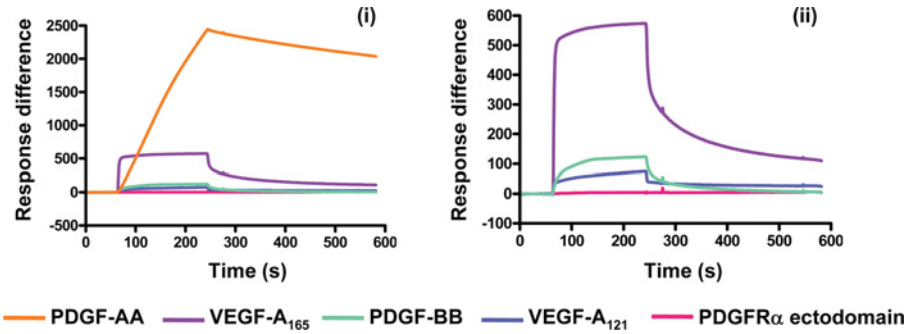

Figure S4 NRP-1 interactions with PDGF ligands and PDGFRα

BIAcore analysis was used to examine the interactions between immobilized recombinant NRP-1 (R&D Systems) and soluble ligands PDGF-AA, PDGF-BB, VEGF-A_{165}, VEGF-A_{121} and a recombinant PDGFRα ectodomain (produced by C. Bayley). Soluble ligands were injected over NRP-1 immobilized on a CM5 chip. The response difference denotes the level of interaction above respective control flow cells. (i) PDGF-AA displayed the highest binding affinity for NRP-1; however, this ligand was difficult to evaluate using BIAcore analysis, due to a high level of interaction with control flow cells [1]. (ii) Smaller response difference scale, showing VEGF-$A_{165,}$ PDGF-BB and VEGF-A_{121} bound to NRP-1 with decreasing affinity, but the PDGFRα ectodomain exhibited no detectable binding. Data shown are representative of three independent experiments.

REFERENCE

1 Goretzki, L., Burg, M. A., Grako, K. A. and Stallcup, W. B. (1999) High-affinity binding of basic fibroblast growth factor and platelet-derived growth factor-AA to the core protein of the NG2 proteoglycan. J. Biol. Chem. **274**, 16831–16837

Received 30 September 2009/25 January 2010; accepted 26 January 2010
Published as BJ Immediate Publication 26 January 2010, doi:10.1042/BJ20091512

BJ www.biochemj.org

Biochem. J. (2010) **427**, 29–40 (Printed in Great Britain) doi:10.1042/BJ20091512

SUPPLEMENTARY ONLINE DATA

Neuropilin-1 regulates platelet-derived growth factor receptor signalling in mesenchymal stem cells

Stephen G. BALL, Christopher BAYLEY, C. Adrian SHUTTLEWORTH and Cay M. KIELTY[1]

Wellcome Trust Centre for Cell-Matrix Research, Faculty of Life Sciences, University of Manchester, Manchester M13 9PT, U.K.

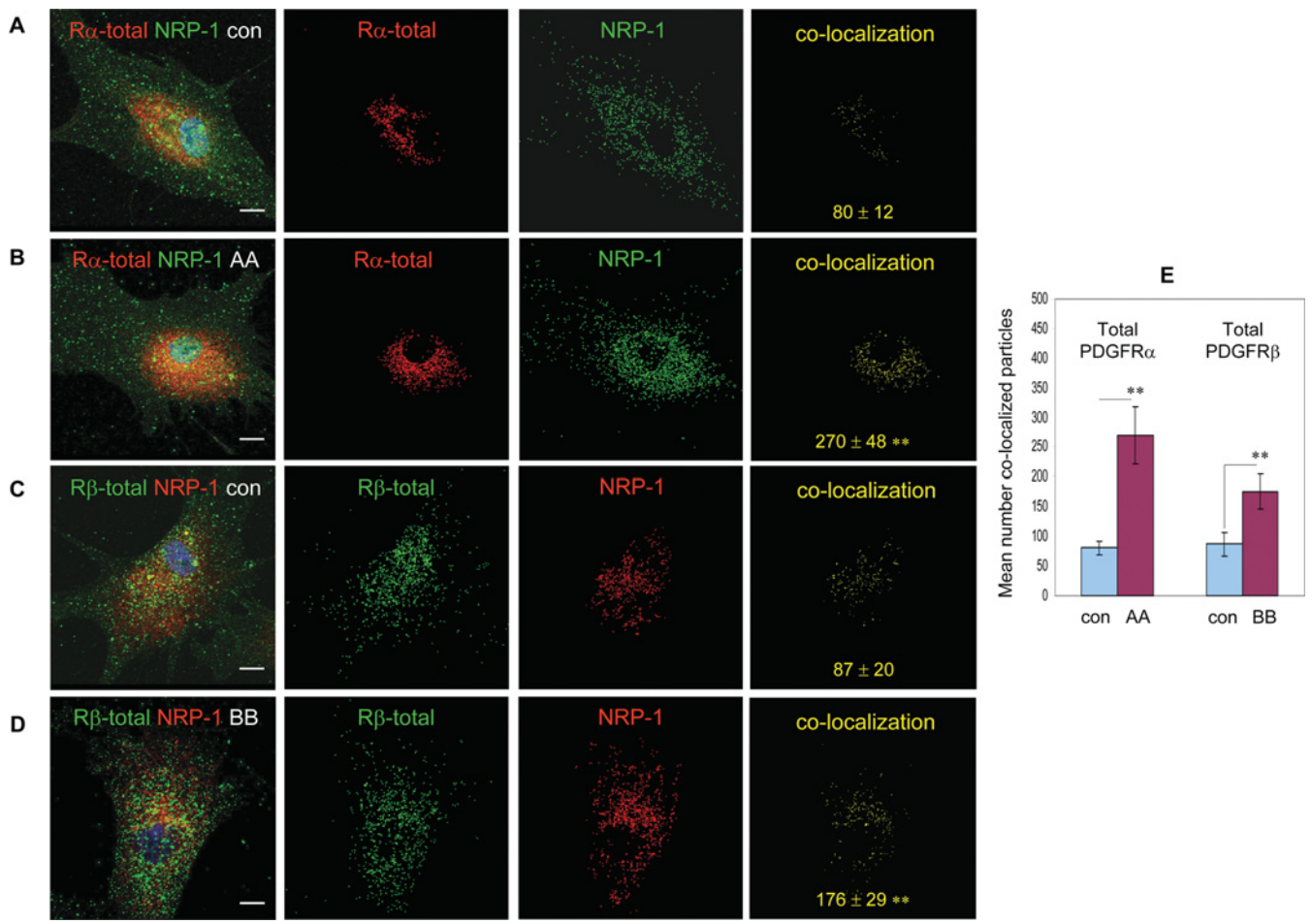

Figure S1 Co-localization of NRP-1 with total PDGFRs

The cellular distribution of NRP-1 and total PDGFRs was examined using pan-PDGFR antibodies. MSCs grown on 0.1% gelatin were cultured for 24 h in serum-free conditions, exposed to PDGF ligands, then co-localization of NRP-1 with either total PDGFRα or PDGFRβ was examined by immunofluorescence microscopy. (**A**) Control unstimulated and (**B**) exposed to 20 ng/ml PDGF-AA for 10 min, showing total PDGFRα (red) and NRP-1 (green). (**C**) Control unstimulated and (**D**) exposed to 20 ng/ml PDGF-BB for 10 min, showing total PDGFRβ (green) and NRP-1 (red). For each image, the corresponding red and green channels having similar threshold values and the same particle size range are shown, together with their co-localization represented by the image in yellow. The mean number of co-localized particles$\pm$S.D. derived from four different single-cell images is denoted in yellow. Nuclei are counter-stained with DAPI (blue). Representative images of at least six independent experiments are shown. Scale bars = 20 μm. (**E**) Histogram showing the ligand-induced increase in co-localization between NRP-1 and total PDGFRα or PDGFRβ, as determined by immunofluorescence analysis. Values are the mean number of co-localized particles$\pm$S.D. derived from six different single-cell images. $^{**}P<0.001$, compared with the corresponding unstimulated control.

[1] To whom correspondence should be addressed (email cay.kielty@manchester.ac.uk).

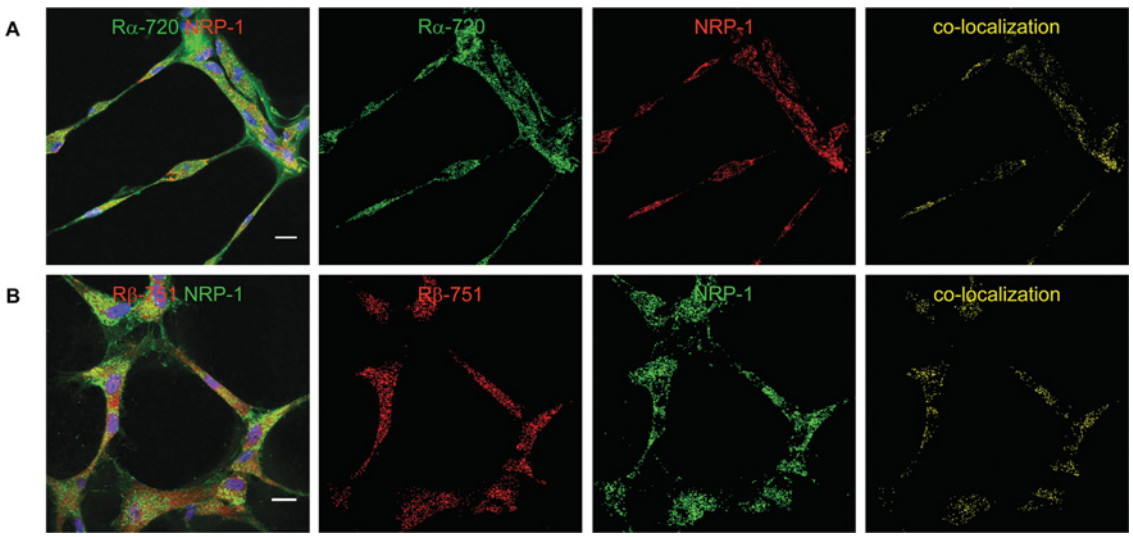

Figure S2 Co-localization of NRP-1 with additional phosphorylated PDGFR sites

The co-localization of NRP-1 with two additional PDGFR phosphorylation sites was examined during the assembly of MSC networks. MSCs were seeded on to Matrigel^{TM} and cultured for 24 h, then co-localization of NRP-1 with either PDGFRα at site Tyr^{720}, or PDGFRβ at site Tyr^{751} was examined by immunofluorescence microscopy. (**A**) MSCs showing PDGFRα-Tyr^{720} (green) and NRP-1 (red). (**B**) MSCs showing PDGFRβ-Tyr^{751} (red) and NRP-1 (green). For each image, the corresponding red and green channels which have similar threshold values and the same particle size range are shown, together with their co-localization represented by the image in yellow. Nuclei are counterstained with DAPI (blue). Representative images of at least four independent experiments are shown. Scale bars = 20 μm.

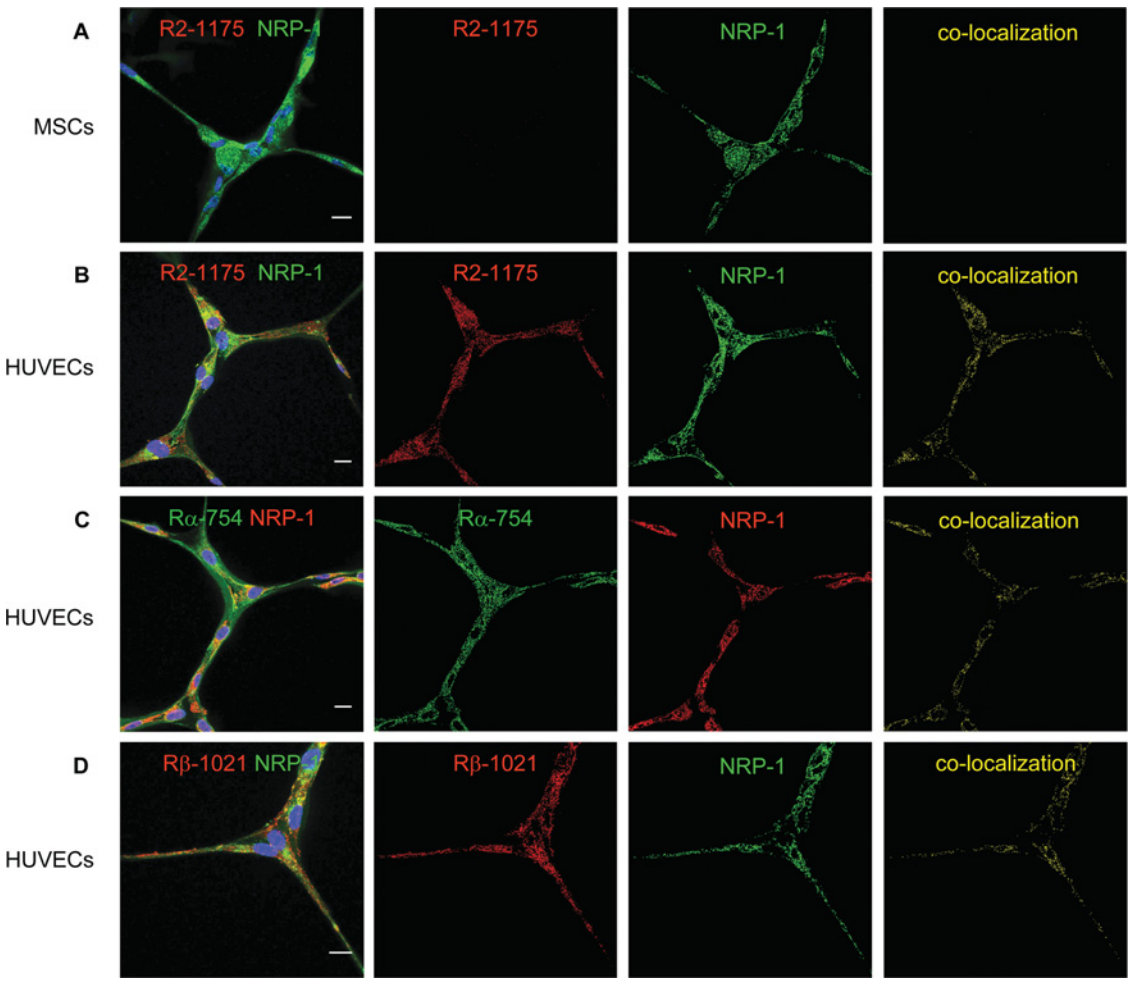

Figure S3 NRP-1 co-localization with PDGFRs in HUVEC networks

The co-localization of NRP-1 and PDGFRs was examined in HUVEC networks. HUVECs or MSCs were seeded on to Matrigel^{TM} and cultured for 24 h, then co-localization of NRP-1 with either VEGFR2 at site Tyr^{1175}, PDGFRα at site Tyr^{754} or PDGFRβ at site Tyr^{1021}, was examined by immunofluorescence microscopy. (**A**) MSCs showing VEGFR2-Tyr^{1175} (red) and NRP-1 (green). (**B**) HUVECs showing VEGFR2-Tyr^{1175} (red) and NRP-1 (green). (**C**) HUVECs showing PDGFRα-Tyr^{754} (green) and NRP-1 (red). (**D**) HUVECs showing PDGFRβ-Tyr^{1021} (red) and NRP-1 (green). For each image, the corresponding red and green channels which have similar threshold values and the same particle size range are shown, together with their co-localization represented by the image in yellow. Nuclei are counterstained with DAPI (blue). Representative images of at least three independent experiments are shown. Scale bars = 20 μm.

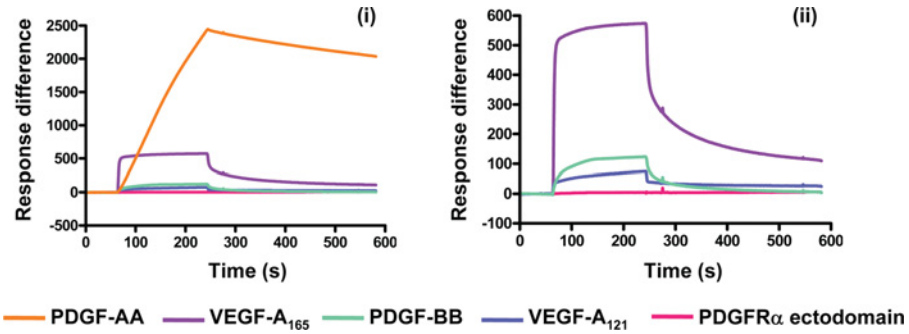

Figure S4 NRP-1 interactions with PDGF ligands and PDGFRα

BIAcore analysis was used to examine the interactions between immobilized recombinant NRP-1 (R&D Systems) and soluble ligands PDGF-AA, PDGF-BB, VEGF-A_{165}, VEGF-A_{121} and a recombinant PDGFRα ectodomain (produced by C. Bayley). Soluble ligands were injected over NRP-1 immobilized on a CM5 chip. The response difference denotes the level of interaction above respective control flow cells. (i) PDGF-AA displayed the highest binding affinity for NRP-1; however, this ligand was difficult to evaluate using BIAcore analysis, due to a high level of interaction with control flow cells [1]. (ii) Smaller response difference scale, showing VEGF-$A_{165,}$ PDGF-BB and VEGF-A_{121} bound to NRP-1 with decreasing affinity, but the PDGFRα ectodomain exhibited no detectable binding. Data shown are representative of three independent experiments.

REFERENCE

1 Goretzki, L., Burg, M. A., Grako, K. A. and Stallcup, W. B. (1999) High-affinity binding of basic fibroblast growth factor and platelet-derived growth factor-AA to the core protein of the NG2 proteoglycan. J. Biol. Chem. **274**, 16831–16837

Received 30 September 2009/25 January 2010; accepted 26 January 2010
Published as BJ Immediate Publication 26 January 2010, doi:10.1042/BJ20091512